Master of Science Thesis

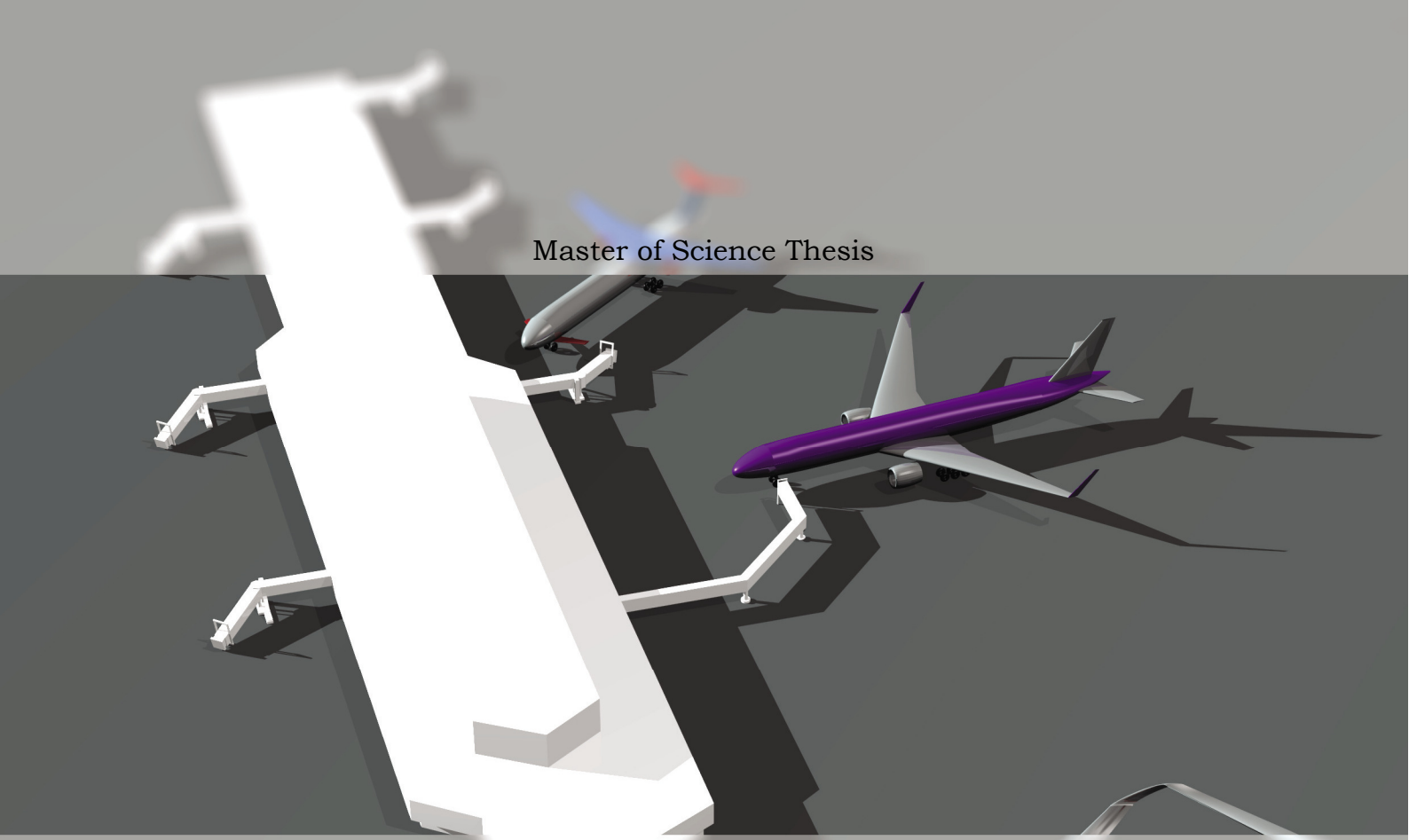

Development of a Wave Drag Prediction Tool for the Conceptual Design Phase

July 14th, 2015

J. Vargas

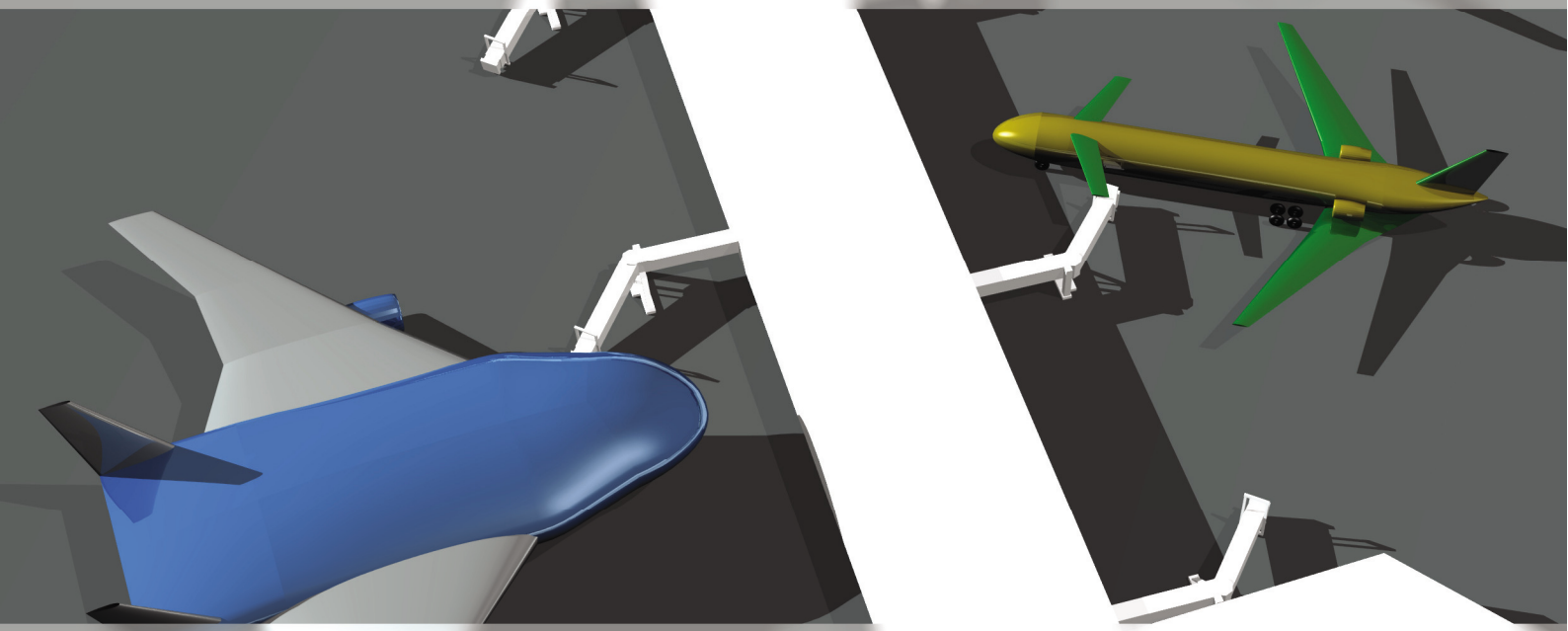

Faculty of Aerospace Engineering - Delft University of Technology

TU Delft Delft University of Technology

Challenge the future

Development of a Wave Drag Prediction Tool for the Conceptual Design Phase

by

Javier Alejandro Vargas Jimenez

In partial fulfillment of the requirements for the degree of

Master of Science
in Aerospace Engineering

Delft University of Technology

July 14th, 2015

Student number:	4257707
Thesis registration number:	033-15-MT-FPP
Supervisor:	Dr. ir. Roelof Vos
Thesis committee:	Dr. Arvind G. Rao
	Dr. Marios Kotsonis

ABSTRACT

The goal of this thesis is to improve the wave drag estimation techniques in the aircraft conceptual design. Based on the most relevant methods, among those developed in the past 60 years, three methods are proposed as an attempt to include more design variables and improve the accuracy of the wave drag prediction. The proposed methods include the use of supercritical airfoils and the cross sectional area distribution of the aircraft as port of the wave drag estimation. The proposed methods are compared to experimental drag data, available in the literature, of four high-subsonic conventional transport aircraft. An accuracy analysis is performed evaluating how well each method predicts the drag divergence Mach number, the wave drag at Mach number 0.8, and how well the predicted curve fitted with the experimental data. The analysis led to the conclusion that the results of the Delta method shows better agreement with the experimental data than the proposed methods.

The state of the art techniques and the proposed methods have been implemented and integrated into a conceptual design tool, as a new module. The module functionality, including its settings, inputs, outputs and functions are also described in this document.

ACKNOWLEDGMENTS

First I would like to express my gratitude to Roelof Vos who has shown a continuous interest as supervisor of this project. His constant support, valuable feedback, useful suggestions and very constructive criticism proved invaluable.

Second I would like to thank the members of my committee: Arvind Rao and Marios Kotsonis, who took the time to asses my work and share their valuable insights.

Third I would like to thank my friends, those who have backed me here, and those who have backed me from all around the world. They have made this time a very enjoyable one.

Finally, a very special thanks to my parents and sister for their unconditional support in pursuing my dreams. They have backed me all the way until here. Without them this would not have been possible.

Contents

List of Figures

List of Tables

NOTATION

Æ	Aspect ratio	(~)
c_{d_w}	Two-dimensional wave drag coefficient	(~)
c_l	Two-dimensional lift coefficient	(~)
C_{D_0}	Zero-lift drag coefficient	(~)
C_{D_L}	Drag due to lift coefficient	(~)
C_{D_P}	Pressure drag coefficient	(~)
C_{D_w}	Wave drag coefficient	(~)
C_L	Lift coefficient	(~)
C_P	Pressure coefficient	(~)
h/c	Airfoil camber	(~)
k_A	Airfoil technological factor, Korn's equation	(~)
$k_{L,w}$	Factors representing spanwise variation of lift and wave drag coefficient	(~)
l/d	Fineness ratio	(~)
L/D	Lift to drag ratio	(~)
M	Mach number	(~)
M_{dd}	Drag divergence Mach number	(~)
M^*	Airfoil technological factor, Torenbeek's equation	(~)
S_{b}	Fuselage base area	(m^2)
S_{max}	Maximum cross sectional area	(m^2)
S_{ref}	Reference area	(m^2)
t/c	Thickness to chord ratio	(~)
$\frac{x_R}{c}$	Rooftop length	(~)
λ	Taper ratio	(~)
ΔM_b	Change in free stream Mach number due to presence of the body	(~)
ΔM_d	Change in free stream Mach number due to design constrains	(~)
$\Lambda_{0,c/4,c/2}$	Sweep angle respect to leading edge, quarter chord and mid chord	(°)
$\overline{\Lambda}_e$	Average equivalent sweep angle	(°)
$\left(\overline{x/c}\right)_e$	Chord-wise location of a line with geometric sweep Λ_e	(~)

Subscripts

2d	Denotes two dimensional flow
3d	Denotes three dimensional flow
DES	Denotes the design point $0.99\,(ML/D)_{\text{max}}$
eL	Effective to the lift coefficient
eM	Effective to the Mach number
ew	Effective to the wave drag coefficient

Abbreviations

MTOW	Maximum take off weight
RMSE	Root mean square error
SC	Supercritical

I

THESIS

1

INTRODUCTION

The development and introduction of the jet engine in the 1950s into commercial airliners opened the possibility of flying higher and faster than previous propulsion technologies. However, the maximum speed of a conventional airliner is usually restricted right below Mach 1, as shown in Figure 1.1. The reason is linked to transonic or compressibility effects such as the development of wave drag. Future long-range airliners may cruise at lower speeds than current models, due to a more environmentally friendly design approach [1].

The study and understanding of the compressibility effects in the transonic regime has been a very active field since the 1950s. As a result, different methods and approaches have been proposed to estimate its effects. These methods can be implemented in different stages of the design. This document will focus on the methods devoted for the conceptual design phase. Additionally, the goal is to link the development of wave drag to the design variables involving wing and fuselage geometry, and the positioning of other elements.

1.1. MOTIVATION

This project has been formulated to improve the current wave drag estimation implemented in the Initiator. The current method is based on a three-dimensional version of Korn's equation an Lock's fourth-power law which includes only few design variables, as described later. As a consequence, an improvement is needed. To satisfy this requirement a first prototype of a wave drag prediction tool should be developed. In contrast to the current method, the tool should be able to warrant design decisions considering the use of supercritical airfoils. Likewise, it should be sensitive to the positioning of elements like nacelles, canards, and the horizontal and vertical tail.

1.2. WAVE DRAG

At high subsonic speeds the local flow in the upper part of the airfoil is likely to have zones of supersonic flow. When the flow has enough supersonic speed, these pockets can end in a shock wave. The loss of total pressure in a shock wave causes wave drag, which becomes very important at high speed flight. Additionally, the adverse pressure gradient on the surface of the airfoil, at the foot of the shock wave, causes thickening and even separation of the boundary layer, leading to a shock induced form drag and an increase in viscous drag. This wave drag is transmitted to the surface of the wing by readjustments in the pressure distribution [1, 2].

A distinction is usually made between wave drag due to volume and wave drag induced by lift. In the first case, it depends on the cross sectional area distribution perpendicular to the flow. The second case is linked to the lift distribution along the wing span. As a result, in the transonic regime the drag coefficient is function of the lift coefficient and the free stream Mach number (M_∞) [1].

Wave drag exists only when flying beyond the *critical Mach number* (M_{crit}), which is defined as the free stream Mach number at which the local Mach number at the minimum pressure point equals the unity for the first time [3]. In a two-dimensional flow, M_{crit} is closely related to the thickness to chord ratio and the lift coefficient. In a three-dimensional flow, M_{crit} is also strongly influenced by other wing parameters like the sweep angle and the aspect ratio [4], as shown in Figure 1.2. When the free stream Mach number exceeds the critical Mach number, the increasing strength of the shock wave and the thickening of the boundary layer often causes a slow increase of the drag coefficient commonly known as *drag creep* [1].

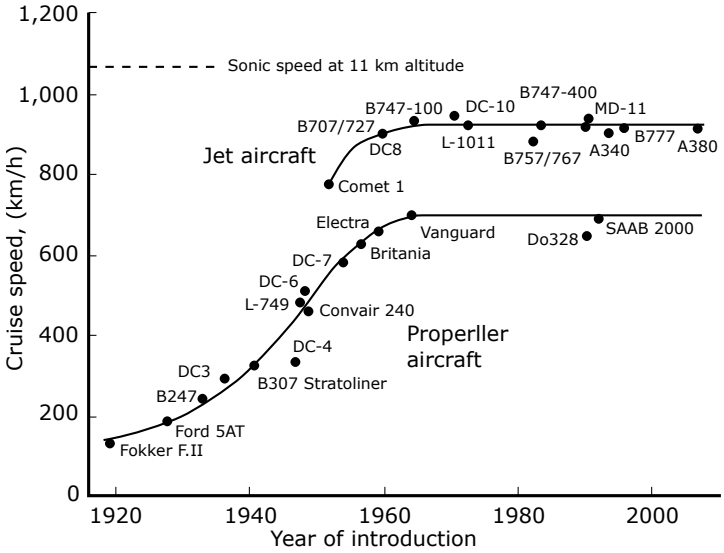

Figure 1.1: Historical development of maximum cruise speed [1]

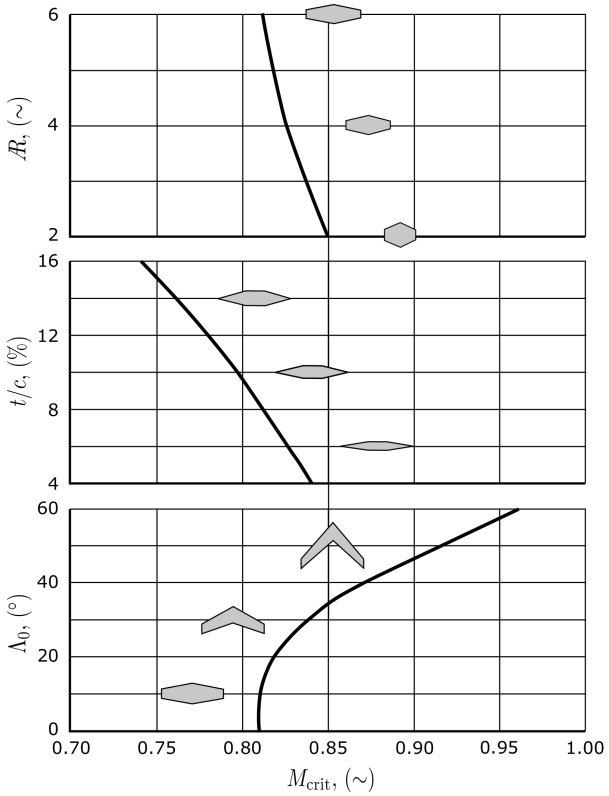

Figure 1.2: Critical Mach number [4]

Flying at even higher Mach numbers can create a rapid drag increment due to the presence of stronger shock waves, flow separation and the associate rise of viscous drag [1, 2]. This situation is commonly described as the *drag divergence Mach number* (M_{dd}). It is an important design parameter for high speed aircraft [1]. As shown in Figure 1.3, the drag divergence Mach number is usually defined at a constant lift coefficient and as the free stream Mach number at which:

- There is an specific increment of drag coefficient ΔC_D respect to an initial value, as shown in Figure 1.3a. The value of ΔC_D is usually 0.002 [1, 5].

- $\partial C_D/\partial M$ has a certain value, as shown in Figure 1.3b. This value is usually 0.1 [1, 5, 6].

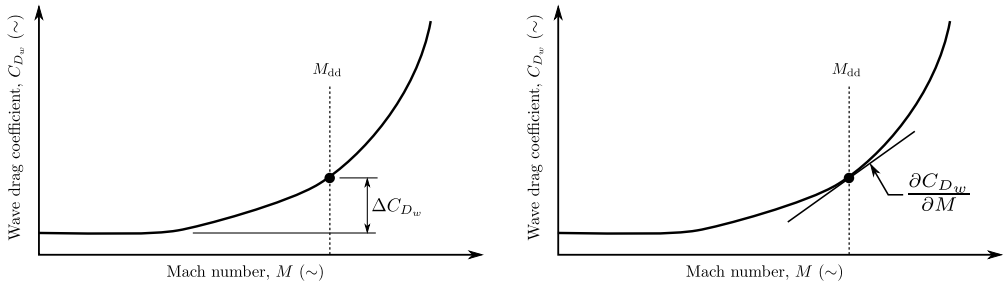

Figure 1.3: Drag divergence boundary definition

The importance of predicting the wave drag comes from the close relation between the drag divergence Mach number and the design point for long-range cruising. Similarly, high-speed cruise is also influenced by compressibility effects. In the transonic regime, wave drag can be accurately predicted using CFD methods. Analytical expressions are still difficult to achieve due to the mixed flow. As a result, experimental data is commonly used to try to estimate these parameters [1].

1.3. STATE OF THE ART

Three handbook methods have been reviewed as starting point for this project including:

- The method currently implemented in the Initiator, which is based on Korn's equation and Lock's fourth-power law.
- The Delta method proposed by Feaguin and Morrison in Reference [7].
- The method proposed by McDevitt in Reference [8] based on NACA 6-series airfoils.

1.3.1. KORN-LOCK METHOD IMPLEMENTED IN THE INITIATOR

The Initiator is an aircraft design tool oriented to the design of conventional and non-conventional configurations based on a set of top-level requirements. It is focused on conventional tube and wing aircraft, three-surface aircraft, prandtl plane, and blended-wing-body aircraft. It has been developed in a modular way using object-oriented programming in MATLAB [9].

The current version of the Initiator uses a wave drag estimation method in two occasions. Both of them based on Equation 1.1, which is a three-dimensional version of Korn's equation [10, 11]. The technological factor, k_A, varies according to the type of airfoil used (conventional or supercritical), or the cruise Mach number. Its application varies as described below.

$$M_{\text{dd}} \cos\Lambda + \frac{\left(\overline{t/c}\right)_w}{\cos\Lambda} + \frac{C_L}{10\cos^2\Lambda} = k_A \tag{1.1}$$

GEOMETRY ESTIMATION - WING

Equation 1.1 is used to estimate the leading edge sweep angle (Λ_0) of the wing at the preliminary sizing phase of the program execution. It is part of the sizing module called *GeometryEstimation* [9], and it is used based on the following:

- The value of M_{dd} is assumed to be equal to $M_{\text{cruise}} + 0.015$
- The term $\left(\overline{t/c}\right)_w$ is defined as the weighted average of the thickness to chord ratio according to the span section. The term is explained in Equation 1.2 where n is the number of sections, and t/c_i and $\frac{y}{b/2}_i$ are the thickness to chord ratio and the position along the semispan, respectively, of each section.
- The lift coefficient, C_L, is obtained as function of the maximum take-off weight (MTOW) obtained from the *Class I Weight Estimation* in an harmonic mission at the design altitude and design Mach number.

$$\left(\overline{t/c}\right)_w = \sum_{i=0}^{n-1} \left[\frac{\frac{t/c_i + t/c_{i+1}}{2}}{\frac{y}{b/2}_{i+1} - \frac{y}{b/2}_i} \right] \tag{1.2}$$

PARASITE DRAG ESTIMATION - WING DRAG

Equation 1.1 is used to estimate the drag divergence Mach number based on wing design parameters obtained after a more design sensitive weight estimation. Then, the critical Mach number is defined as function of the drag divergence Mach number as shown in Equation 1.3a. The wave drag coefficient $\left(C_{D_w}\right)$ is defined as function of the cruise Mach number (M_{cruise}) and the critical Mach number according to Equation 1.3b, commonly know as Lock's fourth-power law [12, 13]. This procedure is part of the analysis module *ParasiteDragEstimation*, and it is used based on the following:

- The lift coefficient, C_L, is calculated by the module `AVLVLM`. In this case the maximum take-off weight (MTOW) resultant from the *Class II Weight Estimation* is used.
- The sweep angle, Λ, is defined as the half chord sweep angle ($\Lambda_{c/2}$).
- The term $\left(\overline{t/c}\right)_w$ is defined as the weighted average of the thickness to chord ratio according to the span section as defined in Equation 1.2.

$$M_{\text{crit}} = M_{\text{dd}} - 0.108 \tag{1.3a}$$

$$C_{D_w} = 20(M_\infty - M_{\text{crit}})^4 \tag{1.3b}$$

1.3.2. DELTA METHOD

It is an empirical drag estimation technique developed by Feaguin and Morrison as a project between Lockheed Corporation and NASA and explained in Reference [7]. It is a expanded version of the method developed previously by Morrison in Reference [14]. The technique is based on experimental data of 19 subsonic and supersonic aircraft and 15 supercritical airfoils. The method is useful in a C_L range between 0.0 and 0.6 and a speed range of $0.2 \leq M \leq 2.0$. It is more appropriate near long-range cruise conditions, but it is not convenient for analyzing turning capabilities or conditions near the maximum lift coefficient [7]. The drag is considered to be composed of two main parts: the part independent of lift $\left(C_{D_{\text{min}}}\right)$, and the lift dependent drag $\left(C_{D_L}\right)$ [7].

$$C_D = C_{D_{\text{min}}} + C_{D_L} \tag{1.4}$$

The zero-lift minimum drag, $C_{D_{\text{min}}}$, consists of friction drag $\left(C_{D_f}\right)$, compressibility drag $\left(\Delta C_{D_C}\right)$ and miscellaneous drag (ΔC_D), as expressed in Equation 1.5a. Likewise, the lift dependent drag, C_{D_L}, is assumed to consist of a theoretical level and an incremental value $\left(\Delta C_{D_P}\right)$ [7], as expressed in Equation 1.5b.

$$C_{D_{\text{min}}} = C_{D_f} + \Delta C_{D_C} + \Delta C_D \tag{1.5a}$$

$$C_{D_L} = \frac{C_L^2}{\pi \mathcal{AR}} + \Delta C_{D_P} \tag{1.5b}$$

From these equations two terms are important for this analysis. The first one is the zero-lift compressibility drag, ΔC_{D_C}. This term is function of the shape and volume effects upon viscous pressure levels due to increases in local Mach numbers, and compressibility effects as local flows become sonic and shock waves form. The zero-lift compressibility drag is divided into three main components as shown in Equation 1.6: compressibility drag due to wing, due to fuselage and due to wing-body interference effects. The last one is assumed to be zero for free stream Mach numbers below one [7].

$$\Delta C_{D_C} = C_{D_{w_{\text{wing}}}} + C_{D_{w_{\text{fus}}}} + C_{D_{\text{int}}} \tag{1.6}$$

The second important term is the incremental value of the lift dependent drag, ΔC_{D_P}, which is mainly function of the wing and includes effects such as boundary layer separation, lift dependent compressibility drag, span-wise flow, and body effects, among others [7]. The procedures to calculate these terms are described below.

DELTA METHOD - ZERO-LIFT WING WAVE DRAG

In the case of the wing wave drag estimation, the method starts by estimating the design lift coefficient $(C_{L_{\text{DES}}})$. In this case, the design point is defined by Morrison in Reference [14] as the Mach numbed and lift coefficient at $0.99\,(ML/D)_{\max}$. The value of $C_{L_{\text{DES}}}$ is estimated using the data shown in Figure 1.4 as function of the aspect ratio, the quarter chord sweep angle and the camber of the wing. The wing camber h/c is the camber at 0.7 of the semi-span of the wing.

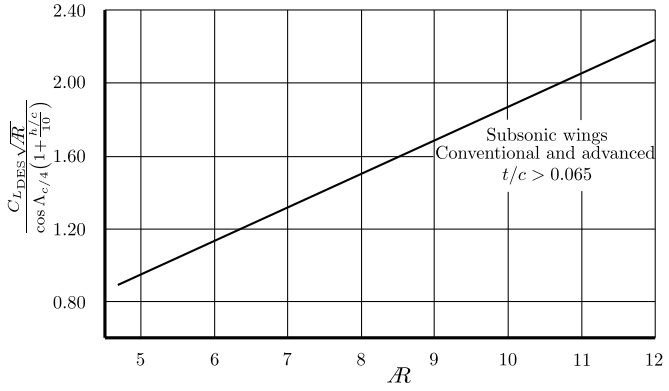

Figure 1.4: Delta method - Design lift coefficient [7]

Then, the two-dimensional drag rise Mach number ($M_{\text{dd 2d}}$) is calculated as function of the design lift coefficient, the type of airfoil, and the effective thickness defined as the wing frontal area divided by the wing planform area. This calculation is performed using Figures 1.5a and 1.5b for advanced and conventional airfoils, respectively. According to Morrison, supercritical, shock-less and peaky airfoils classify as advanced [14].

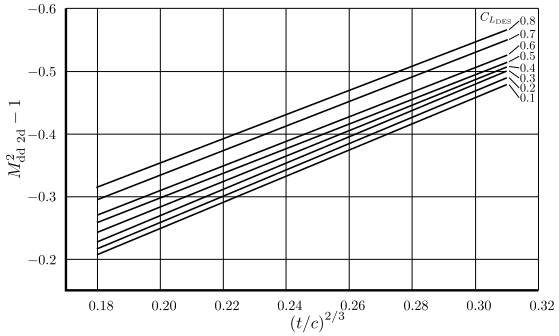

(a) Advanced airfoils

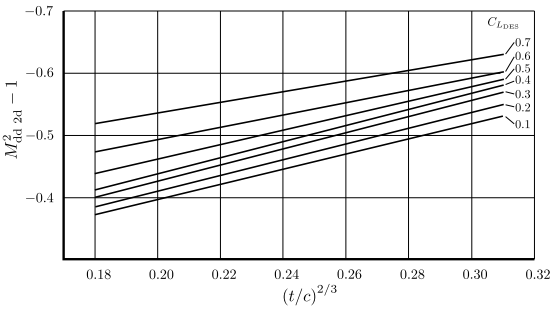

(b) Conventional airfoils

Figure 1.5: Delta method - $M_{\text{dd 2d}}$ [7]

Next, the two-dimensional drag divergence Mach number is transformed into a three-dimensional drag divergence Mach number ($M_{\text{dd 3d}}$). This correction is performed by including the effects of the aspect ratio and the quarter chord sweep angle, from Figures 1.6a and 1.6b, to derive the design Mach number (M_{DES}) according to Equation 1.7 [7].

$$M_{\text{DES}} = M_{\text{dd 3d}} = M_{\text{dd 2d}} + \Delta M_{\Lambda_{c/4}} + \Delta M_{\mathcal{AR}} \tag{1.7}$$

Finally, the wing wave drag coefficient, $C_{D_{w_{\text{wing}}}}$, along the low transonic range is obtained using similar data to that of Figure 1.7. This coefficient is expressed as function of the thickness to chord ratio, the design Mach number, the camber defined at the 70% of the wing span, and the effective thickness [7].

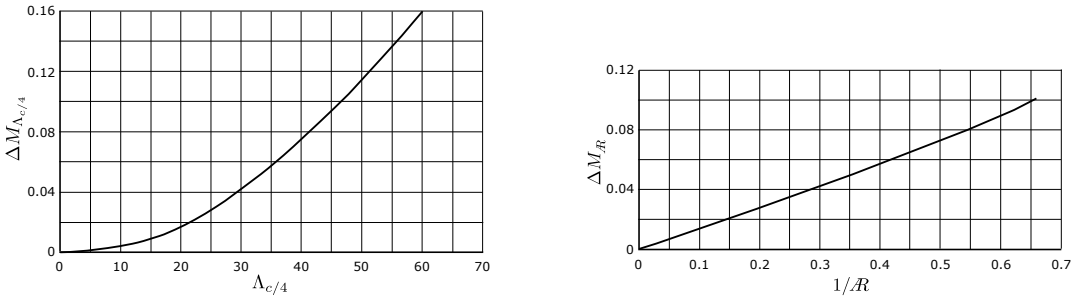

(a) $\Lambda_{c/4}$ correction parameter

(b) $\mathcal{A}R$correction parameter

Figure 1.6: Delta method - $M_{\text{dd 2d}}$ correction parameters [7]

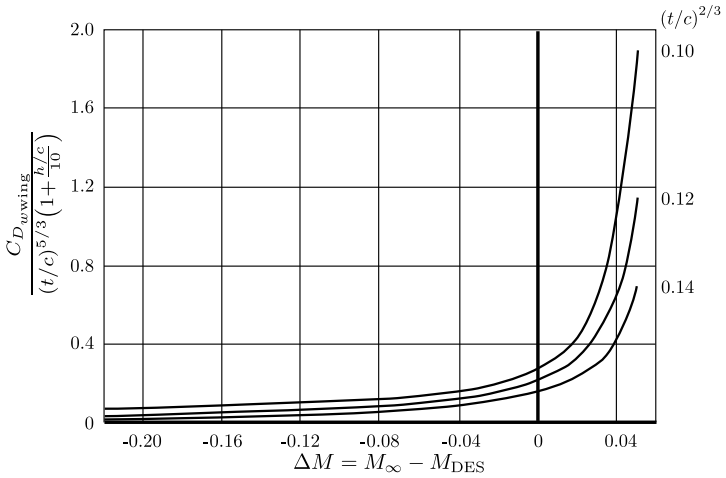

Figure 1.7: Delta Method - Zero-lift wing wave drag [7]

DELTA METHOD - LIFT DEPENDENT WING WAVE DRAG

The portion of wave drag that is dependent of lift, ΔC_{D_P}, can be estimated using similar data to that of Figure 1.8. This coefficient is expressed as function of the thickness to chord ratio, the design Mach number, the design lift coefficient, the camber defined at the 70% of the wing span, and the effective thickness [7].

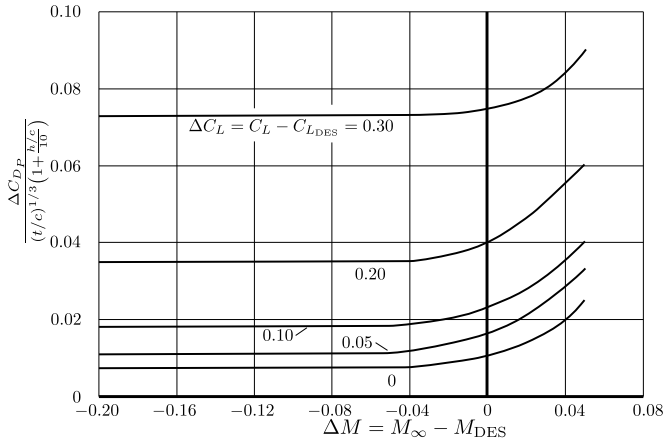

Figure 1.8: Delta method - Lift dependent wing wave drag [7]

DELTA METHOD - FUSELAGE WAVE DRAG

In the case of the fuselage wave drag estimation, the cross sectional area distribution should be obtained including the fuselage, the vertical and horizontal tail surfaces and the nacelles without the engine inlet flow. Then the maximum cross sectional area ($S_{\max}$), the base area (S_b), and the fineness ratio (l/d) are used to estimate the fuselage wave drag coefficient using Figure 1.9. However, as shown in Equation 1.8, the value obtained from this graph has to be corrected according to the reference area. In this case, the reference area is the wing planform area [7].

$$C_{D_{w_{\text{fus}}}} = C_{D\pi}\left(\frac{S_{\max}}{S_{\text{ref}}}\right) \tag{1.8}$$

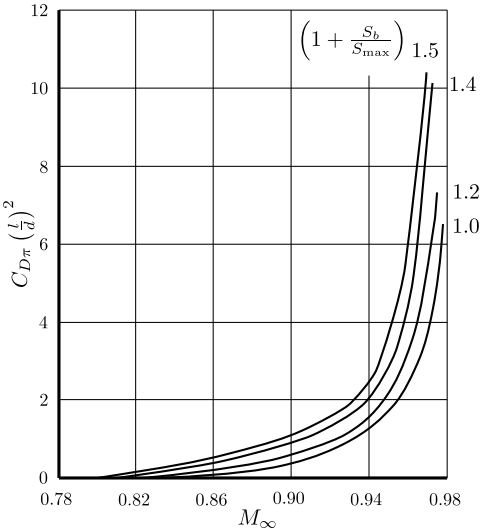

Figure 1.9: Fuselage wave drag [7]

1.3.3. MCDEVITT METHOD

Originally proposed by McDevitt in Reference [8], it is based entirely on experimental data of NACA 6-series airfoils described by Johnson in Reference [15] and explained in the DATCOM [6]. It can be used to estimate the wave drag of a wing with a specific sweep, thickness to chord ratio, aspect ratio, taper and lift coefficient. This method is applicable only for conventional, straight-tapered wings; and it assumes that the friction drag coefficient remains constant in the transonic regime [4, 6].

The method as explained in the DATCOM considers the drag of the aircraft to be formed of two main components, as shown in Equation 1.9: zero-lift drag $\left(C_{D_0}\right)$ and drag due to lift $\left(C_{D_L}\right)$.

$$C_D = C_{D_0} + C_{D_L} \tag{1.9}$$

According to Reference [6], the term C_{D_0} can be divided into two parts: friction drag $\left(C_{D_f}\right)$ and zero-lift wave drag $\left(C_{D_{w_{\text{wing}}}}\right)$, as described in Equation 1.10. In contrast, the term C_{D_L} is not divided into any components but treated as a whole along the transonic regime.

$$C_{D_0} = C_{D_f} + C_{D_{w_{\text{wing}}}} \tag{1.10}$$

MCDEVITT METHOD - ZERO-LIFT WAVE DRAG

The term $C_{D_{w_{\text{wing}}}}$ is focused on the wave drag of the wing under non-lifting conditions and is based on the von Kármán similarity rules. These rules state that the flow pattern over two airfoils must be the same if the value of the term $(t/c)^{1/3}\left|1-M^2\right|$ is the same for each airfoil. As a result, if drag is known for a wing section as a function of Mach number the corresponding quantity for similar sections can be computed by the relation $C_D \propto (t/c)^{5/3}$. The method starts then by estimating the wave drag coefficient of the unswept wing using the data shown in Figure 1.10. If the thickness to chord ratio and the aspect ratio are known, it is

possible to estimate the wing wave drag coefficient of an unswept wing along the transonic range. The wave drag coefficient obtained from this graph has to be transformed to the wave drag coefficient of a swept wing according to the quarter chord sweep angle ($\Lambda_{c/4}$) using Equations 1.11a and 1.11b and the data obtained from Figure 1.10 as fairing. This transformation is entirely based on simple sweep theory [4, 6] and an example can be seen in Figure 1.11.

$$M_{\text{dd}_{\text{swept-wing}}} = \frac{M_{\text{dd}_{\text{unswept-wing}}}}{(\cos\Lambda_{c/4})^{1/2}} \tag{1.11a}$$

$$C_{D_{w_{\text{peak}_{\text{swept-wing}}}}} = C_{D_{w_{\text{peak}_{\text{unswept-wing}}}}} (\cos\Lambda_{c/4})^{2.5} \tag{1.11b}$$

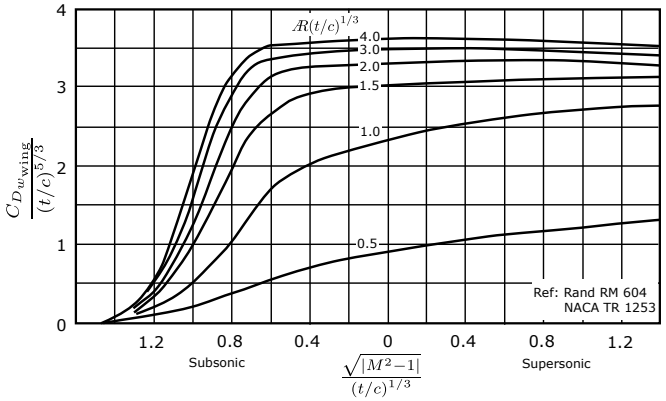

Figure 1.10: Wing transonic drag correlations for unswept wings with NACA 6-series airfoils [6]

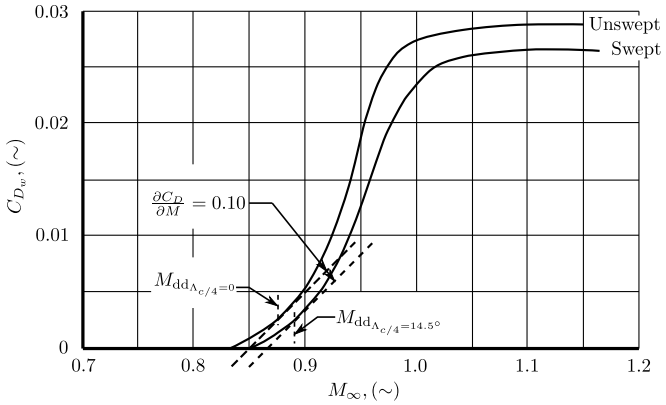

Figure 1.11: McDevitt method - Simple sweep theory [6]

MCDEVITT METHOD - LIFT DEPENDENT DRAG

The second part of the method is focused on estimating the wing drag due to lift, C_{D_L}, in transonic conditions. In this case the wing wave drag is influenced by changes in the flow separation, the development of the boundary layer under lifting conditions, and the interaction between the shock wave and the boundary layer [8]. The correlations are expressed as function of the thickness to chord ratio, the lift coefficient, the aspect ratio and the taper. An example for $\lambda = 1.0$ and $\mathcal{A}\tan\Lambda_0 = 0$ is shown in Figure 1.12. There is experimental data available between $0 \leq \lambda \leq 1$ and $0 \leq \mathcal{A}\tan\Lambda_0 \leq 6$ in Reference [6].

Equivalent taper: Since the aircraft involve in the analysis do not always have straight tapered wings, it is necessary to use the taper of an equivalent wing as defined in Equation 1.12. This geometrical equivalence is based on the area of a trapezoid, similar to the concept proposed in Reference [16].

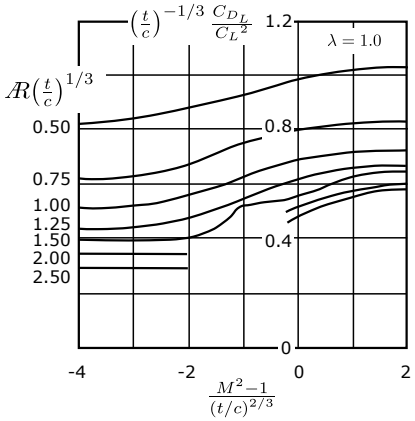

Figure 1.12: Lift dependent wing transonic drag correlations for wings with NACA 6-series airfoils [6]

$$\lambda_{eq} = \frac{c_{tip}}{c_{root_{eq}}} \qquad \text{where} \qquad c_{root_{eq}} = \frac{2S}{b} - c_{tip} \tag{1.12}$$

1.3.4. METHOD ANALYSIS

The methods described before were compared with the experimental data of the following aircraft: an Airbus A320-200, a Boeing 737-800, a Boeing 747-100, and a McDonnell Douglas DC-10-30 [17]. The first two aircraft are equipped with supercritical airfoils, whereas the last two have peaky airfoils. More details of these aircraft as test cases are given in Section 3. Results are shown in Figure 1.13 for a lift coefficient of 0.4.

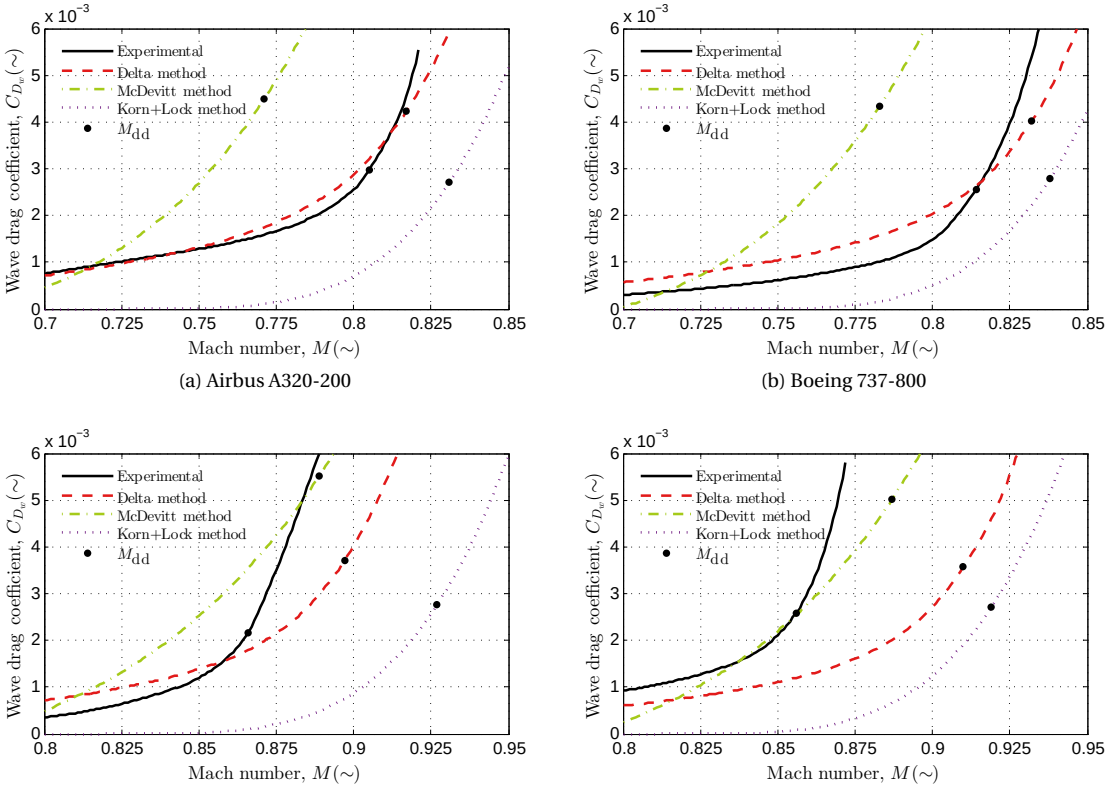

(a) Airbus A320-200

(b) Boeing 737-800

(c) Boeing 747-100

(d) McDonnell Douglas DC-10-30

Figure 1.13: Experimental vs. Handbook methods estimation at $C_L = 0.4$ for four airliners using advanced airfoils. Experimental data obtained from Reference [17]

Figure 1.13 clearly shows how the Korn-Lock method overestimates the development of wave drag, and does not estimate any drag creep. In contrast, the Delta method does estimate the drag creep more accurately. This is especially true for the two aircraft equipped with supercritical airfoils: the Airbus A320-200 and the Boeing 737-800, whose estimations are shown in Figures 1.13a and 1.13b, respectively. The estimated M_{dd} using the Delta method for these two aircraft is also closer to the experimental data than the estimations of the other methods. On the other hand, the estimated drag divergence Mach number of the aircraft equipped with peaky airfoils, shown in Figures 1.13c and 1.13d, using the McDevitt method is closer to the experimental data than the estimations of the other methods. However, the wave drag development of the method proposed by McDevitt is more gradual than that of the experimental data.

The disagreement observed in the methods previously described also justifies the need for an improved procedure to estimate the wave drag of an aircraft in transonic conditions. This is also aligned with the motivation described previously in Section 1.1.

1.4. RESEARCH QUESTION AND OBJECTIVE

The motivation and the analysis of the methods described in state of the art lead to the following main objective:

To improve the wave drag prediction of fixed wing aircraft at low transonic conditions in the conceptual design phase.

It should be possible to predict wave drag around lifting and non lifting bodies and to compare the results with a well documented test case. Some differences can be observed between the methods described in the state of the art. These differences involve also the data and theories on which these methods are based. This leads to the following question:

Is it possible to improve the wave drag prediction methods by including more design variables, or by adapting them to the current technologies and aircraft specifications?

In this project, the methods to predict wave drag refer to the procedures that are able to estimate the wave drag of a body flying at low transonic conditions, while including conceptual design variables and flight conditions.

SPECIFIC OBJECTIVES

In order to accomplish the main goal of this project, the following set of sub objectives has been formulated:

- To fully implement the more relevant methodologies found in the literature, and to validate them using test cases previously defined.
- To clearly identify the most reliable methods from the information obtained in the validation process and taking into account the following considerations:
  - Are these methods sensitive to the design variables and flight conditions?
  - Are these methods computationally inexpensive?
  - To what extend do these methods cope with the interference effects between wings and nacelles, as well as between horizontal and vertical tail?
  - To what extend are these methods useful to analyze variables such as the type of airfoil, the wing sweep or fineness ratios of the fuselage and nacelles? Or to analyze elements such as wing body fairings?
  - Which are the main assumptions made when using these methods?
- To fully incorporate and integrate the developed tool into the Initiator.
- To fully document the process and the code for future users and potential improvements of the tool.

2

PROPOSED METHODS

As observed in the previous section, the Korn-Lock method currently implemented in the Initiator does not predict the wave drag of an aircraft with good accuracy. In general, some of the methods described in the state of the art fail to predict the drag creep or the drag divergence Mach number accurately. This shows that there are opportunities of improving the procedures described. This Chapter shows the three methods proposed to enhance the wave drag estimation. Some extra assumptions are also discussed.

2.1. PROPOSED METHOD A

The first proposed method involves modifying the parameters used in the Delta method to correct the two-dimensional drag divergence Mach number ($M_{\text{dd 2d}}$) to a three-dimensional drag divergence Mach number ($M_{\text{dd 3d}}$). The original parameters were shown previously in Figure 1.6, as proposed by Feaguin and Morrison in Reference [7] for the Delta method. As described in Section 1.3.2, the values obtained from these graphs are function of the wing sweep and aspect ratio and are added directly to the previously estimated $M_{\text{dd 2d}}$ to obtain $M_{\text{dd 3d}}$ using Equation 1.7. The result obtained is the base of the subsequent calculations in which the wing wave drag is estimated as function of the thickness to chord ratio and the camber [7].

IMPROVED THREE-DIMENSIONAL CORRECTION FOR SWEPT WINGS

To improve the correction of the predicted $M_{\text{dd 2d}}$ to $M_{\text{dd 3d}}$, Equation 2.1 is used instead. This equation is part of a more extended set of correlations presented in Reference [2] and allows one to include more design parameters in the procedure. The three main terms of Equation 2.1 are explained below.

$$M_{\text{dd 3d}} = M_{\text{dd 2d}} \sec \Lambda_{eM} - (\Delta M_b + \Delta M_d) \tag{2.1}$$

Effective sweep angle - Λ_{eM} The first term, Λ_{eM}, is the effective sweep angle relevant to the Mach number. According to Reference [18], Λ_{eM} is defined as the sweep angle of an infinite constant-chord wing which gives the same drag-rise behavior as the mid-semi-span portion of the real wing, when both have the same stream-wise thickness to chord ratio and same thickness distribution.

The effective sweep angle, Λ_{eM}, can be calculated as function of the thickness to chord ratio, the wing sweep, the taper, and the upper surface pressure distribution of the airfoil. The pressure distribution is represented in the calculations by the length of the rooftop (x_R/c) of the upper surface pressure distribution, as shown in Figure 2.3. The procedure starts with dividing Λ_{eM} into two main components, as shown in Equation 2.2.

$$\Lambda_{eM} = \overline{\Lambda}_e + \Delta\Lambda_e \tag{2.2}$$

First, the average equivalent sweep over a range of stream-wise thickness to chord ratios $\left(\overline{\Lambda}_e\right)$ can be obtained according to Equation 2.3, where $(\overline{x/c})_e$ is the chord-wise location of a line having a geometric sweep equal to Λ_e.

$$\tan \overline{\Lambda}_e = \tan \Lambda_0 - 2\left(\tan \Lambda_0 - \tan \Lambda_{c/2}\right)(\overline{x/c})_e \tag{2.3}$$

Similarly, $(\overline{x/c})_e$ is expressed in Equation 2.4. In this case the term $\Delta(\overline{x/c})_e$ is the contribution to $(\overline{x/c})_e$ due to sweep and taper. The values of $\left[(\overline{x/c})_e - \Delta(\overline{x/c})_e\right]$ and $\Delta(\overline{x/c})_e$ can be calculated as function of the rooftop length, the sweep and the taper using the data of Figures 2.1a and 2.1b, respectively.

$$(\overline{x/c})_e = \left[(\overline{x/c})_e - \Delta(\overline{x/c})_e\right] + \Delta(\overline{x/c})_e \tag{2.4}$$

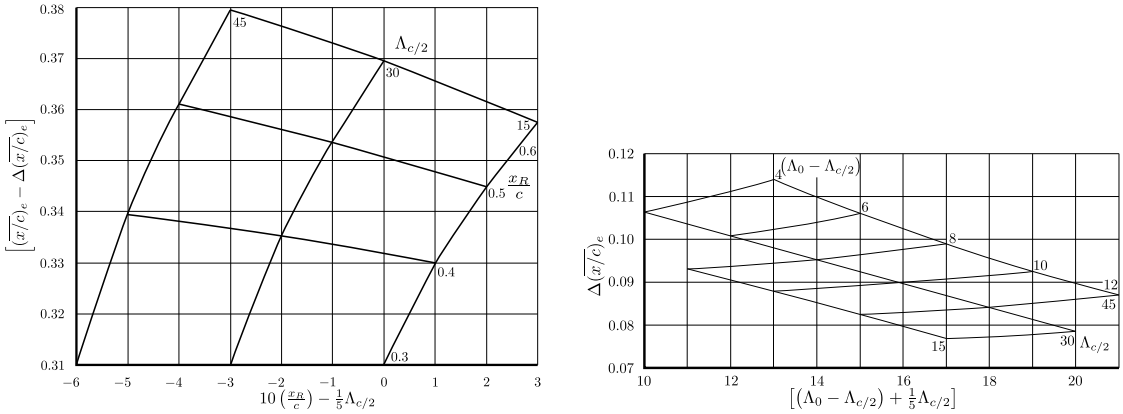

Figure 2.1: Chord-wise location of equivalent sweep [18]

Secondly, the correction $(\Delta\Lambda_e)$ can be calculated graphically as function of the thickness to chord ratio, the rooftop length, and the taper using data similar to that of Figure 2.2. In this case, there is data available for values of x_R/c between 0.3 and 0.6.

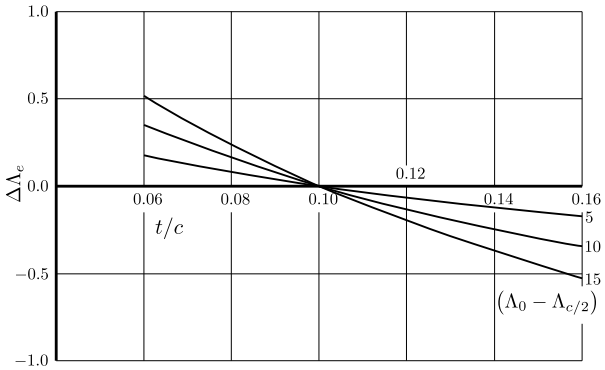

Figure 2.2: Correction of the average equivalent sweep $(x_R/c = 0.6)$ [18]

Rooftop length of the upper surface pressure distribution It is assumed that the pressure distribution of the upper surface of the airfoil has a particular form at the drag rise condition. This form consists of a level plateau (flat rooftop) extending from the immediate vicinity of the leading edge to a given station along the chord (x_R) [19]. An example of a flat plateau in the pressure distribution of a supercritical airfoil is shown in Figure 2.3. If the length of the rooftop is unknown, it can be estimated as function of the two-dimensional drag divergence Mach number, the thickness to chord ratio and the lift coefficient by using the experimental data presented in Reference [19]. There is data available within the following ranges:

$$0.3 \leq x_R/c \leq 0.6$$

$$0.06 \leq t/c \leq 0.18$$

$$0.60 \leq M_{\text{dd}} \leq 0.85$$

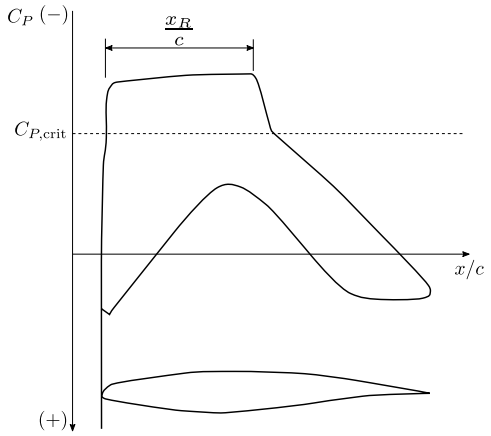

Figure 2.3: Rooftop definition

Increment in the Mach number due to body presence - ΔM_b The second term of Equation 2.1 is ΔM_b, which accounts for the increment of the free stream Mach number in the upper-surface of the wing due to the body in the presence of a wing. For a wing of low aspect ratio ΔM_b can be as high as 0.020, whereas for high aspect ratio wing it can be as low as 0.010. A high wing layout can decrease the value of ΔM_b by 0.005 and a low wing layout can increase its value by the same amount [2].

Increment in Mach number due to design constrains - ΔM_d The third term of Equation 2.1 is ΔM_d. It is related to the design constrains that potentially lead to the generation of wave drag. This means that for wings of modest sweep angles ($\Lambda_{c/2}$ up to 20°) the value of ΔM_d is negligible if no major design changes were needed to avoid the development of premature supercritical flow. For higher wing sweep values, where the occurrence of premature supercritical flow has not been possible to avoid, the value of ΔM_d is as large as 0.04 [2].

2.2. PROPOSED METHOD B

When employed to predict the wave drag of wings with supercritical airfoils, the McDevitt method described in Section 1.3.3 tends to underestimate the drag divergence Mach number (M_{dd}). To overcome this issue, the drag divergence Mach number predicted by Torenbeek's equation, described below, is employed as a reference point to shift the predicted curve. The principle is shown in Figure 2.4. This allows one to correct the predictions of the McDevitt method described in Section 1.3.3 when used to estimate the wave drag of wings equipped with advanced airfoils. The estimation of the fuselage wave drag is done based on procedure given in the Delta method as described in Section 1.3.2.

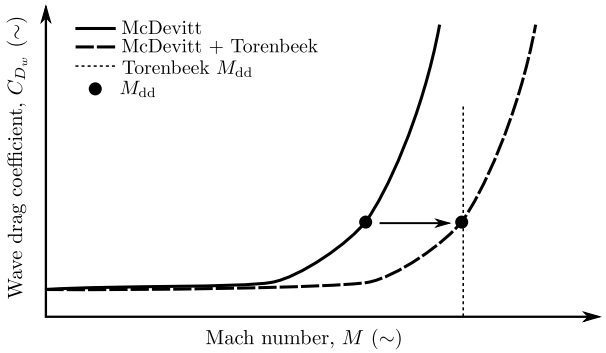

Figure 2.4: Main principle of Proposed method B

TORENBEEK'S EQUATION

A three-dimensional adaptation of a modified Korn's equation [11] is proposed by Torenbeek in Reference [1] and shown in Equation 2.5.

$$M_{\text{dd}} \cos\Lambda_{c/2} + \frac{\left(\overline{t/c}\right)_w}{\cos\Lambda_{c/2}} + 0.10\left\{\frac{1.1C_L}{\cos^2\Lambda_{c/2}}\right\}^{1.5} = M^* \tag{2.5}$$

The coefficient M^* is defined for supercritical airfoils as 0.935. The term $\left(\overline{t/c}\right)_w$ refers to the average thickness to chord ratio weighted for the span as described previously in Equation 1.2, C_L is the design lift coefficient, and $\Lambda_{c/2}$ refers to the outboard mid-chord sweep angle. The factor 1.1 accounts for the higher than average aerodynamic loading of the outboard wing [1, 20].

2.3. PROPOSED METHOD C

Similar to the correlations proposed by McDevitt for NACA 6-series airfoils in Reference [8], a set of correlations is created based on the experimental data of various supercritical airfoils. The airfoils included have a thickness to chord ratio of 0.10, 0.14 and 0.17 as given by Harris in References [21–23] and by Ferris in Reference [24]. A correlation curve is obtained for each airfoil, which includes the thickness to chord ratio (t/c), the wave drag coefficient $\left(c_{d_w}\right)$, the lift coefficient (c_l), and the Mach number (M). The correlations are based on the following function:

$$\frac{c_{d_w}}{(t/c)^{1/3}\, {c_l}^2} = f\left(\frac{\sqrt{1-M^2}}{(t/c)^{1/6}}, t/c\right) \tag{2.6}$$

Each correlation curve is the result of the optimization of a parametric Bézier curve such that, when transformed according to Equation 2.6, it estimates the two-dimensional wave drag coefficient with a high level of accuracy. An example of these estimations is presented in Figure 2.5. These graphs show the experimental and estimated values of c_{d_w}, at different c_l values, along the Mach range available for the supercritical airfoil with t/c equal to 0.14. The experimental data is obtained from Reference [22]. The same procedure is performed for the other two airfoils. The three resultant correlations are shown in Figure 2.6. In contrasts to the correlations proposed by McDevitt and presented in Figures 1.10 and 1.12, there are no independent correlations for the zero-lift and the lifting conditions. As in the previous proposed method, the estimation of the fuselage wave drag is done based on the procedure of the Delta method as described in Section 1.3.2.

The correlations of Figure 2.6 can be used to obtain the wave drag of an airfoil, given the values of t/c, c_l, and M along the low transonic range. The value of t/c is defined as the average value weighted according to the span sections, as previously shown in Equation 1.2. The two-dimensional lift coefficient, c_l, is obtained from the three-dimensional lift coefficient, C_L, using a procedure given in Reference [2] and explained below.

CORRECTION FROM TWO- TO THREE-DIMENSIONAL FLOW

The framework given in Reference [2] is used for transforming the two-dimensional coefficients into three-dimensional coefficients. As mentioned in Section 2.1, using this framework allows one to include more design variables into the procedure than the simple sweep theory. In this case, the framework is used for converting C_L into c_l, c_{d_w} into C_{D_w}, and $M_{2\text{d}}$ into M_∞.

Transforming the lift coefficient The two-dimensional lift coefficient, c_l, is needed as one of the inputs of the correlations of Figure 2.6. Its value is obtained from the three-dimensional lift coefficient, C_L, using Equation 2.7 from Reference [2].

$$C_L = k_L c_l \cos^2\Lambda_{eL} \tag{2.7}$$

Equation 2.7 includes two main terms. The first term k_L is proportional to the ratio between the local lift coefficient and the total wing lift coefficient at the spanwise section where the basic airfoil is incorporated to the wing. It is usually in the range between 0.8 to 0.9 [2].

The second term Λ_{eL} of Equation 2.7 is the effective sweep angle relevant to the lift coefficient and it is assumed to be equal to $\Lambda_{c/4}$ [2].

Transforming the wing wave drag coefficient Figure 2.6 allows one to estimate the value of the two-dimensional wave drag coefficient, c_{d_w}. Then, it is transformed into a three-dimensional coefficient, C_{D_w}, by using Equation 2.8 also from Reference [2].

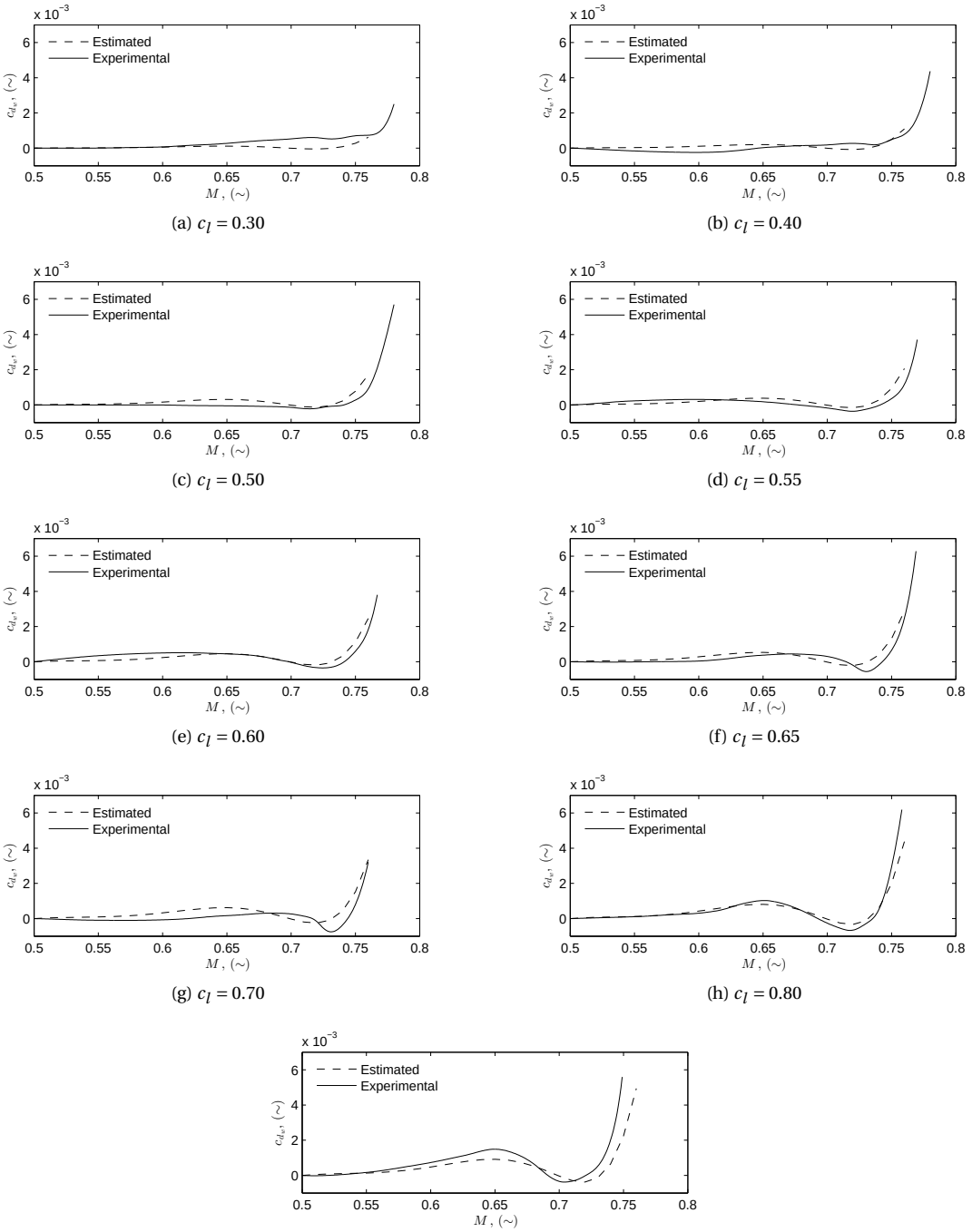

(a) $c_l = 0.30$

(b) $c_l = 0.40$

(c) $c_l = 0.50$

(d) $c_l = 0.55$

(e) $c_l = 0.60$

(f) $c_l = 0.65$

(g) $c_l = 0.70$

(h) $c_l = 0.80$

(i) $c_l = 0.85$

Figure 2.5: Estimated vs. experimental c_{d_w} for a supercritical airfoil of $t/c = 0.14$ (Experimental data from Reference [22])

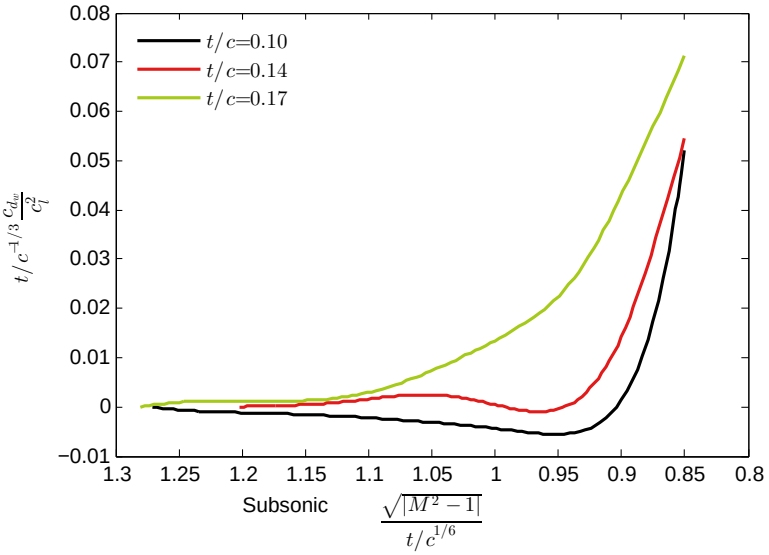

Figure 2.6: Supercritical airfoils two-dimensional correlations

$$C_{D_w} = k_w c_{d_w} \cos^3 \Lambda_{ew} \tag{2.8}$$

Equation 2.8 also includes two main terms. The first term is k_w which accounts for the variation of wave drag across the span. If the initial drag rise is generated in a section that has a high degree of equivalence to the basic section the value of k_w is slightly lower than the unity. Otherwise it is higher than the unity.

The second term of Equation 2.8 is Λ_{ew}, which is the effective sweep angle relevant to the wave drag coefficient. According to Reference [2] it is equivalent to the average for the sweep of the shock front close to drag rise conditions. In the absence of that information it can be assumed to be equal to $\Lambda_{c/2}$.

Transforming the free stream Mach number The results of Figure 2.6 relate the two-dimensional wave drag coefficient to a two-dimensional Mach number. This Mach number can be transform into its three-dimensional equivalent by using Equation 2.9 from Reference [2].

$$M_{3\mathrm{d}} = M_{2\mathrm{d}} \sec \Lambda_{eM} + (M_{2\mathrm{d}} - M_{\mathrm{dd\,2d}}) \sec \Lambda_{ew} - (\Delta M_b + \Delta M_d) \tag{2.9}$$

Equation 2.9 has five main terms. The term Λ_{ew} was just described as part of the transformation of the wave drag coefficient. The terms Λ_{eM}, ΔM_b, and ΔM_d have been already described in Section 2.1. The term $M_{\mathrm{dd\,2d}}$ is the two-dimensional drag divergence Mach number and is determined by using also a two-dimensional boundary, as described next.

Transforming the drag divergence boundary To calculate the value of the two-dimensional drag divergence Mach number, $M_{\mathrm{dd\,2d}}$, a two-dimensional boundary $\partial c_d / \partial M_{2\mathrm{d}}$ is needed. Equation 2.10, from Reference [2], can be used for such purpose. Equation 2.10 has two main terms: k_w, and Λ_{ew}. Both of them have been described before as part of Equation 2.8.

$$\frac{\partial C_D}{\partial M_{3\mathrm{d}}} = k_w \frac{\partial c_d}{\partial M_{2\mathrm{d}}} \cos^4 \Lambda_{ew} \tag{2.10}$$

2.4. OTHER ASSUMPTIONS

The methods described in Section 1.3 and the methods proposed in this chapter are focused mainly in conventional configurations. However, the Initiator is currently able to analyze some non-conventional configurations, as already mentioned in Section 1.3.1. As a result, the following assumptions are proposed:

Firstly, in the case of three-surface aircraft, the canard can be included as part of the cross sectional area distribution similar to the horizontal stabilizer. The main wing is still considered to be the driving surface

concerning the generation of wave drag. In that case the cross sectional area distribution would look similar to that of Figure 2.7

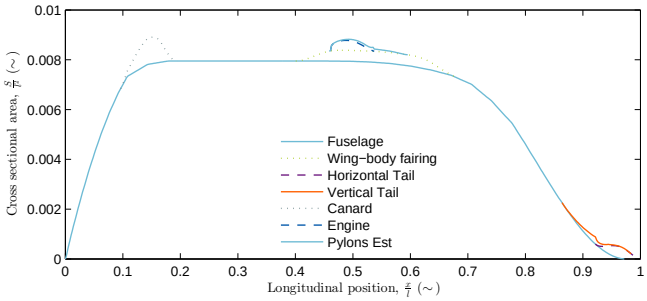

Figure 2.7: Cross sectional area distribution of three-surface aircraft

Additionally, in the case of a prandtl plane, both wings, namely the front and the rear wing, are considered to be the main sources of wave drag. In this case, the value of C_{D_w} of each wing is based on the respective wing planform area. They have to be corrected to the total planform area $S_{ref_{\text{Total}}}$, defined in Equation 2.11a, by using equations 2.11b and 2.11c. For the rear wing, or in general for forward swept wings, it is assumed that the effects caused by the forward sweep are the same as those caused by the back sweep. One has to be cautious with this assumption, especially when using more elaborated frameworks to transform the two-dimensional coefficients into the equivalent three-dimensional coefficients. Frameworks such as the one used in the methods A and C, not only consider the equivalent sweep of a wing but also the interaction between the wing and body. The interaction between wing and body of a forward sweep configuration can be slightly different to that of a common aft sweep configuration. Figure 2.8, from Reference [11], shows the difference in the drag polar between a forward sweep and an aft sweep configuration.

$$S_{ref_{\text{Total}}} = S_{ref_{\text{Front wing}}} + S_{ref_{\text{Rear wing}}} \tag{2.11a}$$

$$C_{D_{w_{\text{Front wing}}}} = C'_{D_{w_{\text{Front wing}}}} \frac{S_{ref_{\text{Front wing}}}}{S_{ref_{\text{Total}}}} \tag{2.11b}$$

$$C_{D_{w_{\text{Rear wing}}}} = C'_{D_{w_{\text{Rear wing}}}} \frac{S_{ref_{\text{Rear wing}}}}{S_{ref_{\text{Total}}}} \tag{2.11c}$$

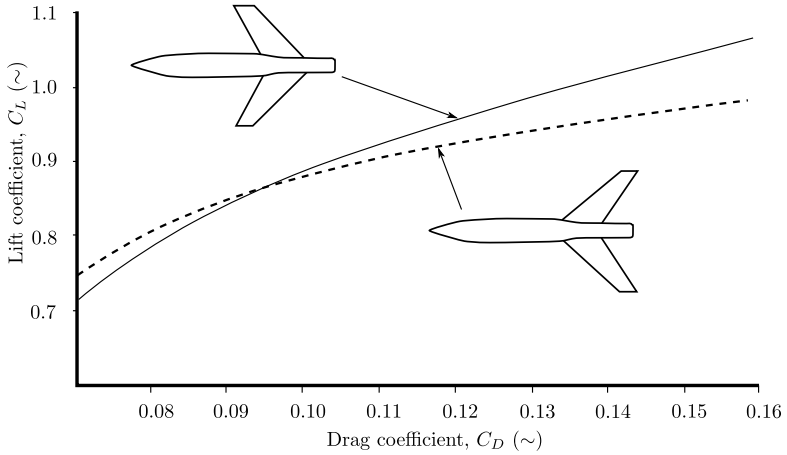

Figure 2.8: Forward/Aft sweep wing drag comparison, $M_\infty = 0.9$ [11]

2.5. SUMMARY

The three methodologies proposed in this project have been briefly described in this section. All the methods show a strong influence of the wing in the development of wave drag. A summary of the variables included in

each method is shown in Table 2.1. The Delta method was also included in the summary as reference, since it is the method that exhibits the best agreement among those described in the state of the art in Section 1.3. This information, in addition to the accuracy analysis described in the next Chapter, can be used to determine the most suitable procedure to estimate the wave drag in the conceptual design phase.

Table 2.1: Variables included in each proposed method

	Wing								Airfoil type		Fuselage		
	$\mathcal{AR}$	Λ	λ	t/c	h/c	C_L	$\frac{x_R}{C}$	Wing Layout	SC	Conv.	$S_{\max}$	S_b	l/d
Method A	✓	✓	✓	✓	✓	✓	✓	✓	✓	✓	✓	✓	✓
Method B	✓	✓	✓	✓	✗	✓	✗	✗	✓	✓	✓	✓	✓
Method C	✓	✓	✓	✓	✗	✓	✓	✓	✓	✗	✓	✓	✓
Delta Method	✓	✓	✗	✓	✓	✓	✗	✗	✓	✓	✓	✓	✓

3

TEST CASE DEFINITION

This Chapter focuses on the test cases, additional functions and other considerations needed to validate the estimations of the proposed methods. Section 3.1 describes the test cases used to validate the methods proposed in the previous section.Finally, the methods used to calculate the cross sectional area distribution and to estimate some of the surfaces of the aircraft are explained in Section 3.2.

3.1. TEST CASES

3.1.1. AIRCRAFT GEOMETRY

Four aircraft were used as test cases for validation purposes, namely: the Airbus A320-200, the Boeing 737-800, the Boeing 747-100, and the McDonnell Douglas DC-10-30. The first two are short- to medium-range aircraft, and the last two are long-range aircraft. The experimental data of these four aircraft is given by Obert in Reference [17]. The data needed to recreate the geometry of the aircraft in the Initiator was also extracted from Obert [17], whereas the data regarding the fuselage and other surfaces dimensions was obtained using Jane's [25]. Table 3.1 shows a summary of the basic data required by the Initiator to recreate the geometry and specifications of each aircraft.

Table 3.1: Aircraft geometry

		Airbus A320-200	Boeing 737-800	Boeing 747-100	McDonnell Douglas DC-10-30	Units
FUSELAGE						
Length		37.57	38.02	68.55	51.97	(m)
Diameter		4.14	3.76	6.50	6.02	(m)
WINGS						
Root chord		7.08	8.76	16.40	13.93	(m)
Thickness to chord ratio	*Root*	0.18	0.18	0.15	0.14	(~)
	Kink	0.12	0.11	0.10	0.09	(~)
	Tip	0.11	0.11	0.08	0.08	(~)
Quarter chord sweep	*Inboard*	21.1	30.0	37.5	33.00	(°)
	Outboard	25.0	25.5	39.5	35.00	(°)
Taper	*Inboard*	0.53	0.55	0.56	0.57	(~)
	Outboard	0.44	0.29	0.42	0.38	(~)
Span		34.09	34.32	59.60	50.39	(m)
Aspect Ratio		9.39	9.45	6.90	6.91	(~)
Kink position at semi-span		0.38	0.29	0.42	0.37	(~)
Type of airfoil		Supercritical			Peaky	
SPEED						
Cruise Mach number		0.78	0.785	0.84	0.82	(~)

3.1.2. EXPERIMENTAL DATA

The drag coefficient (C_D) at different lift coefficients for the four aircraft mentioned before was obtained from Reference [17] and is shown in Figure 3.1. To obtain the wave drag coefficient, it is assumed that the friction drag and theoretical induced drag remain constant along the transonic range, and the wave drag corresponds to the increment respect to the initial value at Mach number equal to 0.6, as show in the scheme of Figure 3.2. This assumption is aligned with the procedures described in Sections 1.3 and 2.

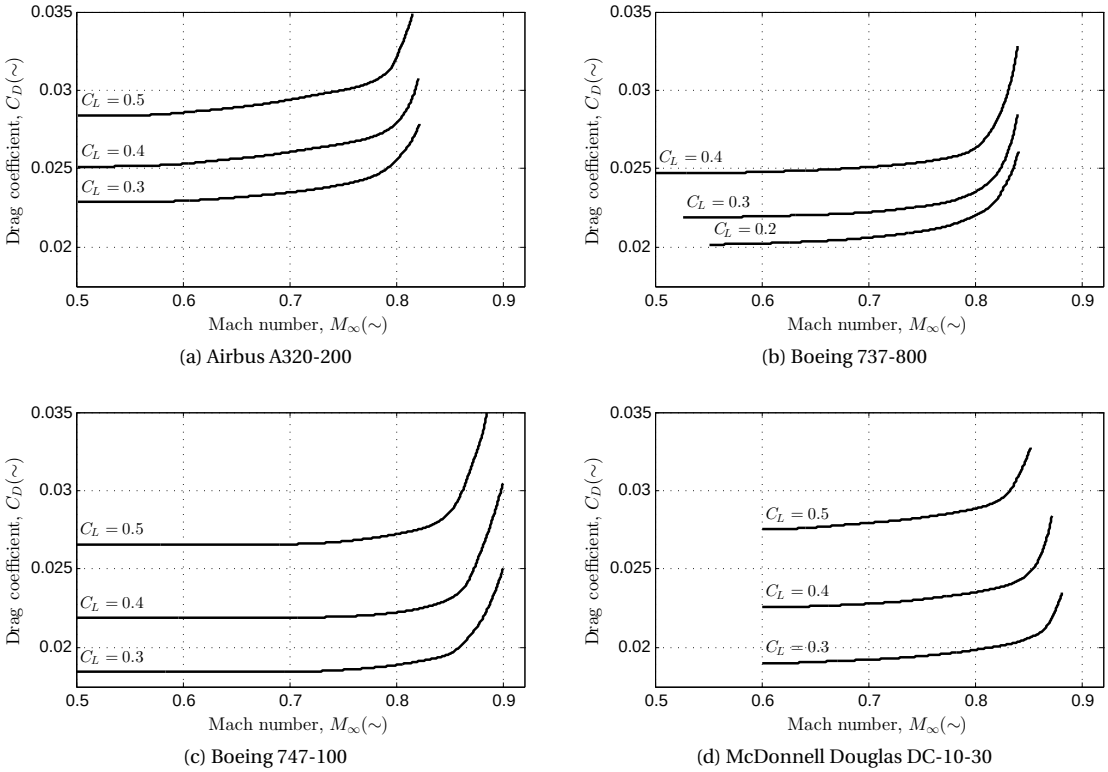

(a) Airbus A320-200

(b) Boeing 737-800

(c) Boeing 747-100

(d) McDonnell Douglas DC-10-30

Figure 3.1: Experimental drag coefficient for four airliners using advanced airfoils [17]

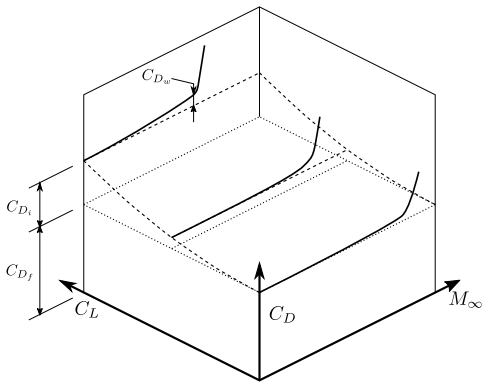

Figure 3.2: Assumptions regarding definition of wave drag

The Airbus A320-200 and the Boeing 737-800 have very similar transonic characteristics. They have a very similar wing area but different thickness to chord ratio. The similarities in drag characteristics can be understood as the high quality of both designs [17]. The use of supercritical airfoils in the Boeing 737-800 allowed higher long-range cruise Mach numbers, compared to previous designs. However, their lower wing sweep corresponds with their earlier drag rise characteristics, especially when compared to the long-range airliners included in the analysis. In the case of the Boeing 747-100, the drag rise characteristics do not worsen when

increasing C_L [17]. This proves that different airfoil shapes can influence the dependency of the drag divergence Mach number to the lift coefficient [26]. However, the same cannot be said in the case of the McDonnell Douglas DC-10-30 since the lift coefficient clearly affects the drag rise behavior. Compared to the Boeing 747-100, the McDonnell Douglas DC-10-30 has a lower wing sweep. However, this might be compensated with the slightly thinner airfoils.

3.2. AREA DISTRIBUTION

As part of the fuselage wave drag estimation described in Section 1.3.2 and used in all the proposed methods, it is necessary to calculate the maximum cross sectional area distribution (S_{max}) and the base area (S_b). In this case, neither the inlet capture area nor the wings should be included. However, the horizontal and vertical tail surfaces should be included [7]. To calculate these values the following surfaces are included:

- Surfaces generated by the Initiator:
  - Fuselage
  - Vertical tail(s)
  - Horizontal tail
  - Engine(s)
  - Canard
- Estimated surfaces:
  - Wing-body fairing
  - Engine pylons

3.2.1. GENERATED SURFACES

Currently, the Initiator is able to generate a set of three-dimensional coordinates that represent some of the surfaces of an aircraft. The coordinates are organized in arrays of x, y and z coordinates which allow them to be easily sorted into groups. The coordinates and the groups that form a common vertical tail are represented by the red dots and the blue lines, respectively, in the example of Figure 3.3.

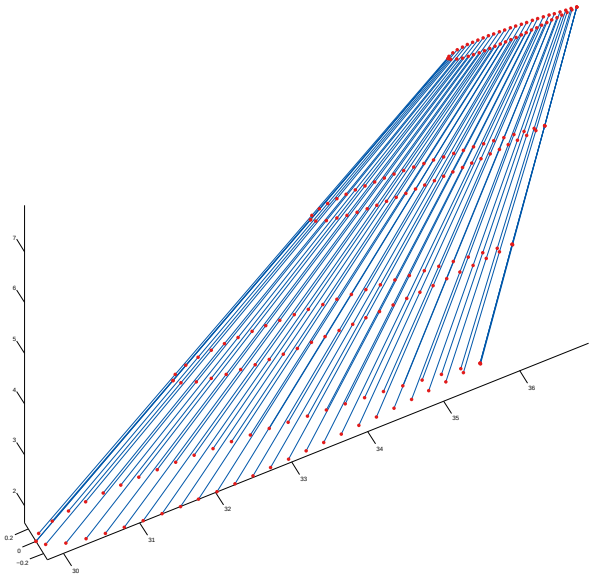

Figure 3.3: Surface definition example

After obtaining the three-dimensional coordinates of a surface, they are divided into left and right. This is shown in Figure 3.4a, where the fuselage and the horizontal tail left surfaces are represented in red and blue respectively. Then, the intersection between the surfaces is calculated to subtract the extra sections as

shown in Figure 3.4b. The MATLAB code `SurfaceIntersection` [27] is used to obtain the intersections of the surfaces listed below:

- Horizontal tail with fuselage or with vertical tail (depending on the horizontal tail position).
- Vertical tail with fuselage.
- Canard with fuselage.

Finally, the cross sectional area distribution of each surface is calculated separately as shown in the example in Figure 3.4c. In this Figure, the black points represent the intersection of a vertical plane, at an arbitrary station x, with the horizontal tail surface. The area enclosed by these points is the cross sectional area of the surface at a specific body station. This procedure is executed for the left and right sides of the surfaces mentioned before.

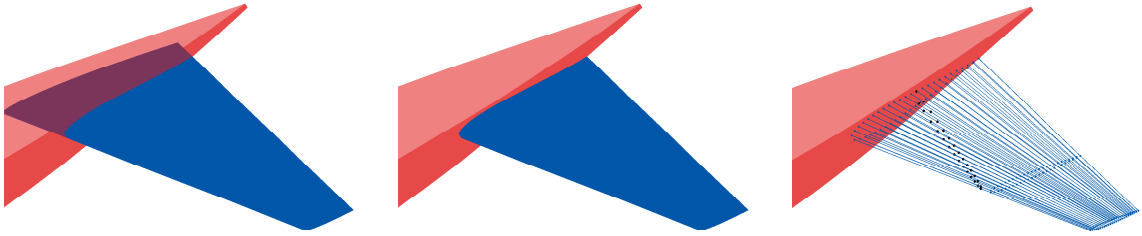

(a) Initial surface (b) Intersected surface (c) Cross sectional area

Figure 3.4: Area distribution procedure

3.2.2. ESTIMATED SURFACES

The Initiator does not include any geometry of the nacelle pylons and wing-body fairing yet. To compensate for their absence in the calculations of the cross sectional area distribution, they are estimated as described below.

WING-BODY FAIRING ESTIMATION

The cross sectional area distribution of the wing-body fairing is estimated according to two parameters: the wing-body fairing proportions, and the cross sectional area distribution of a known case. Firstly, it is assumed that the wing-body fairing can be represented by a semicircular body similar to that of Figure 3.5a. This body has a radius r and the length of the three sections is defined as a function of that radius by the variables a, b and c. The cross sectional area distribution of such body can easily be calculated, and an example is shown in Figure 3.5b.

Next, the cross sectional area of a Boeing 747, as given in Figure 3.6, is taken into account. This data allows one to determine the values of a, b and c, as follow: from Figure 3.6, it is estimated that the length of the first and third section of the wing-body fairing is almost the same, and that the length of the medium section is equivalent to 1.76 times that of the front section. In other terms:

$$a = c$$

$$b = 1.76 \times a$$

From Figure 3.6, one can also see that the maximum cross sectional area of the wing-body fairing is about 16% of the area of the fuselage cylindrical part, without counting the cab. Since the diameter of the fuselage is known, it is possible to estimate the value of the maximum cross sectional area of the wing-body fairing, and consequently of r. It is also assumed that the length of the mid section,$b \times r$, corresponds with the length of the chord of the wing at the intersection between the wing and the fuselage. This assumption leads to a good estimation of b and the other two variables. The resultant values for a, b and c, are 6.25, 11, 6.25, respectively.

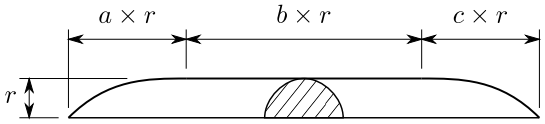

(a) Example of wing-body fairing dimensions (Modified from Reference [28])

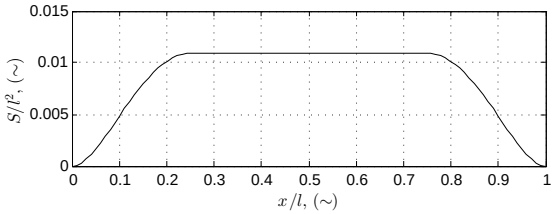

(b) Example of wing-body fairing cross sectional area distribution

Figure 3.5: Wing-body fairing estimation

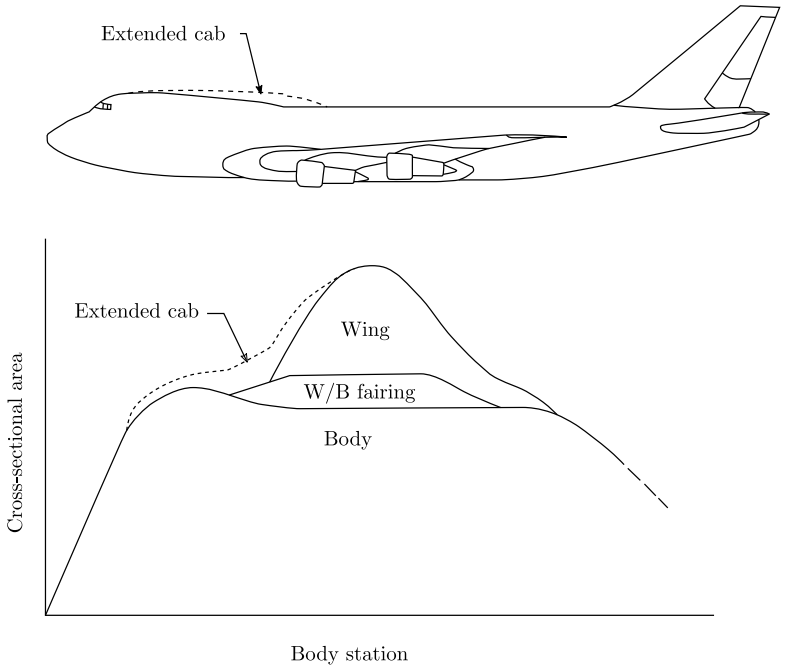

Figure 3.6: Boeing 747 area distribution [29]

PYLON ESTIMATION

A purely geometrical estimation of the engine pylons was included too. It is based on the geometrical shape of a compression pylon airfoil of thickness to chord ratio equal to 0.20, as shown in Figure 3.7. This profile was obtained from a similar profile presented in Reference [30], and it is also settable. In the case of wing-mounted nacelles, the airfoil is projected from the lower part of the wing to the upper external part of the nacelle. The result is a pylon with a shape similar to that represented by the solid line of Figure 3.8. The chord of the pylon $\left(c_{\text{pylon}}\right)$ is related to both the length of the nacelle and the local chord of the wing at the spanwise position of the engine.

To estimate the cross sectional area (S) at a station x (represented in Figure 3.8 by the filled area) the projection of the airfoil on the vertical intersection plane (represented in Figure 3.8 by the thick dashed line) is used. The thickness distribution of this projection is defined by the following equation:

$$t'\left(x'_a\right) = t\left(x_a\right) \tag{3.1}$$

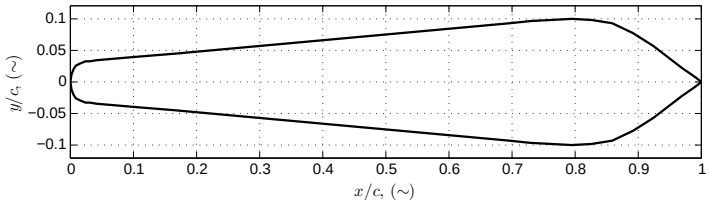

Figure 3.7: Compression airfoil geometry based on Reference [30]

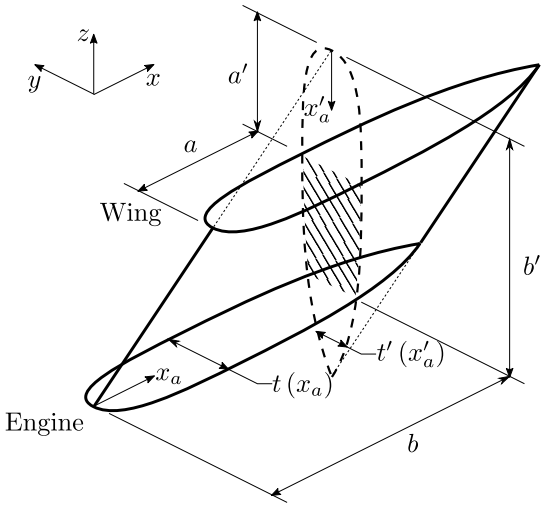

Figure 3.8: Estimation of the cross sectional area distribution of a pylon

where x_a is an auxiliary variable defined in the range $0 \leq x_a \leq c_{\text{pylon}}$ and $x'_a = x_a m_{\text{pylon}}$. The term m_{pylon} is defined by the following equation:

$$m_{\text{pylon}} = \frac{\Delta z_{\text{le}}}{\Delta x_{\text{le}}} = \frac{z_{\text{le@wing}} - z_{\text{le@engine}}}{x_{\text{le@wing}} - x_{\text{le@engine}}} \tag{3.2}$$

From Figure 3.8 and Equation 3.1 it is also possible to see that the cross sectional area $S(x)$ can be expressed as the following integral:

$$\begin{aligned} S(x) &= \int_{a'}^{b'} t'\left(x'_a\right) dx'_a \\ &= \int_{a'}^{b'} t\left(x_a\right) dx'_a \\ &= \int_{a}^{b} t\left(x_a\right) m_{\text{pylon}} dx_a \end{aligned} \tag{3.3}$$

where $a' = a m_{\text{pylon}}$ and $b' = b m_{\text{pylon}}$. The terms a and b are also function of x, as follow:

$$a = \begin{cases} 0 & \text{if } x_{\text{le@engine}} \leq x \leq x_{\text{le@wing}} \\ x - x_{\text{le@wing}} & \text{if } x_{\text{le@wing}} < x \end{cases} \tag{3.4}$$

$$b = \begin{cases} x - x_{\text{le@engine}} & \text{if } x_{\text{le@engine}} \leq x \leq x_{\text{te@engine}} \\ c_{\text{pylon}} & \text{if } x_{\text{te@engine}} < x \end{cases} \tag{3.5}$$

$$\tag{3.6}$$

Then, a more general expression would be:

$$S(x) = \int_{a(x)}^{b(x)} t\left(x_a\right) m_{\text{pylon}} dx_a \qquad \left(x_{\text{le@wing}} \leq x \leq x_{\text{te@engine}}\right) \tag{3.7}$$

From the term m_{pylon} it is clear that this expression tends to infinity when the pylon is aligned with the vertical axis; in other words, when it has no sweep. In this case, the cross sectional area can be expressed as:

$$S(x) = \Delta z_{\text{le}}\, t(x) \qquad (x_{\text{le}} \leq x \leq x_{\text{te}}) \tag{3.8}$$

In the case of a fuselage-mounted engine, the value of m_{pylon} is given as a settable, and is defined by Equation 3.9. The values of $x_{\text{le@fuselage}}$ and $y_{\text{le@fuselage}}$ are function then of m_{pylon}, the position and diameter of the nacelle, and a value indicating how much the pylon penetrates the fuselage. This last value is also settable. The rest of the procedure is the same as described before for the wing-mounted engines. The two cases are represented in the schemes of Figure 3.9.

$$m_{\text{pylon}} = \frac{\Delta y_{\text{le}}}{\Delta x_{\text{le}}} = \frac{y_{\text{le@fuselage}} - y_{\text{le@engine}}}{x_{\text{le@fuselage}} - x_{\text{le@engine}}} \tag{3.9}$$

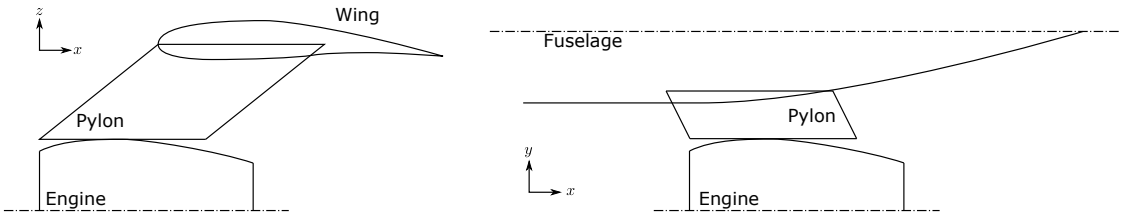

(a) Wing-mounted engine (b) Fuselage-mounted engine

Figure 3.9: Pylon estimation scheme

3.2.3. EXAMPLE OF CROSS SECTIONAL AREA DISTRIBUTION

After estimating the cross sectional area distribution of the most relevant parts of an aircraft, it can be included in the fuselage wave drag estimation described in previous sections. An example of such esimation can be observed in Figure 3.10.

(a)

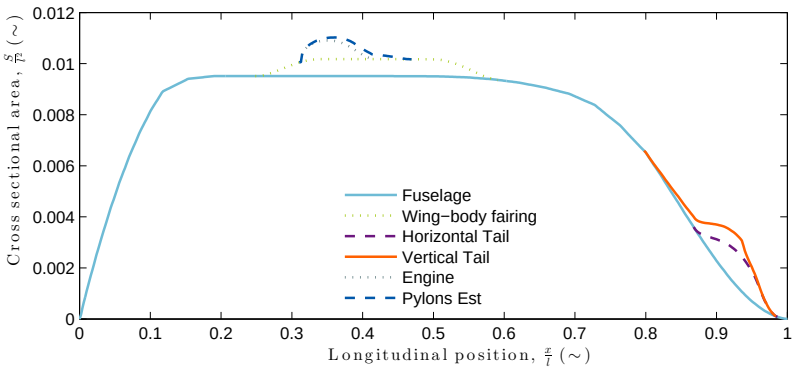

(b)

Figure 3.10: Cross sectional area distribution

4

RESULTS

This Chapter is focused on presenting and analyzing the results of the estimations of the wave drag coefficient. Section 4.1 shows the validation of the estimation of the wave drag coefficients using the methods proposed in Section 2. A brief description of the limitations of this study is included in Section 4.2. An accuracy analysis of each method is performed in Section 4.3; then, a discussion of such analysis is presented. Section 4.4 closes this Chapter showing a comparison between the most accurate method of those analyzed in this document, and the method currently implemented in the Initiator which was explained in Section 1.3.1.

4.1. VALIDATION OF RESULTS

All the methods explained in Section 2 were validated using the four aircraft described in Section 3. Additionally, the Delta method, described in the Section 1.3.2, was also included in this analysis. The results of the estimations of the four aircraft, for each of the lift coefficient (C_L) values available, are shown in Figures 4.1 to 4.4. The points in the graphs correspond to the drag divergence Mach number, M_{dd}, defined by the boundary $\partial C_D/\partial M = 0.1$.

4.2. STUDY LIMITATIONS

This study is focused on two types of conventional aircraft: the short- to medium-range Airbus A320-200, and Boeing 737-800, and the long-range Boeing 747-100 and McDonnell Douglas DC-10-30. As shown previously in Section 3.1, these models are well documented and their geometry can be defined in the Initiator.

It is important to mention that the current capabilities of the Initiator do not allow the generation of the *hump* in the fuselage of the Boeing 747-100. This difference in the geometry leads to a different cross sectional area distribution in the forward section of the aircraft. However, as mentioned in the Section 1.3.2, the method used to estimated the wave drag coefficient of the fuselage takes into account the base area and the maximum cross sectional area. The information given in Figure 3.6, from Reference [29], shows that the maximum cross sectional area distribution, without including the wings, occurs near the wing-body fairing. This is reinforced by adding the cross sectional area of nacelles and pylons, which are almost at the same longitudinal position as the wing-body fairing. As a result, it is expected that the absence of the *hump* will not alter the estimations of the wave drag coefficient of the fuselage.

Unfortunately, due to the absence of experimental data there is not any non-conventional configuration in this analysis. In any case, in Section 2.4 some assumptions and considerations are made concerning the implementation of the methods for the wave drag estimation of non-conventional configurations, as part of any future analysis.

4.3. ACCURACY ANALYSIS

In order to quantify the quality of the predictions of each method, three measurements were used:

- The absolute error $\left|e_{M_{\text{dd}}}\right| = \left|M_{\text{dd}_{\text{exp}}} - M_{\text{dd}_{\text{est}}}\right|$ is used to measure how precise the methods predict the drag divergence number, defined by $\partial C_D/\partial M = 0.1$. A graphical explanation is given in Figure 4.5 and results are shown in Figure 4.7.

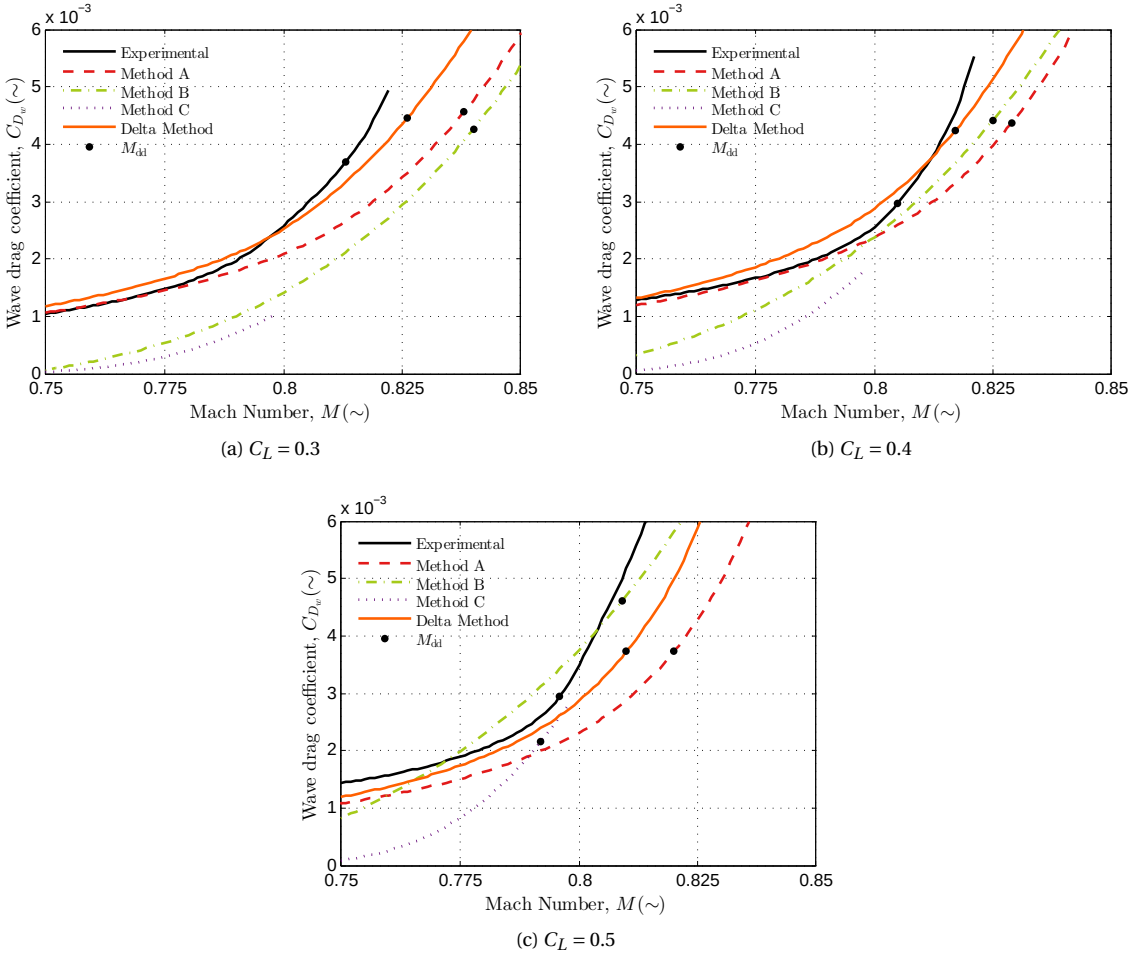

(a) $C_L = 0.3$

(b) $C_L = 0.4$

(c) $C_L = 0.5$

Figure 4.1: Experimental C_{D_w} of the Airbus A320-200 [17] compared to estimated data

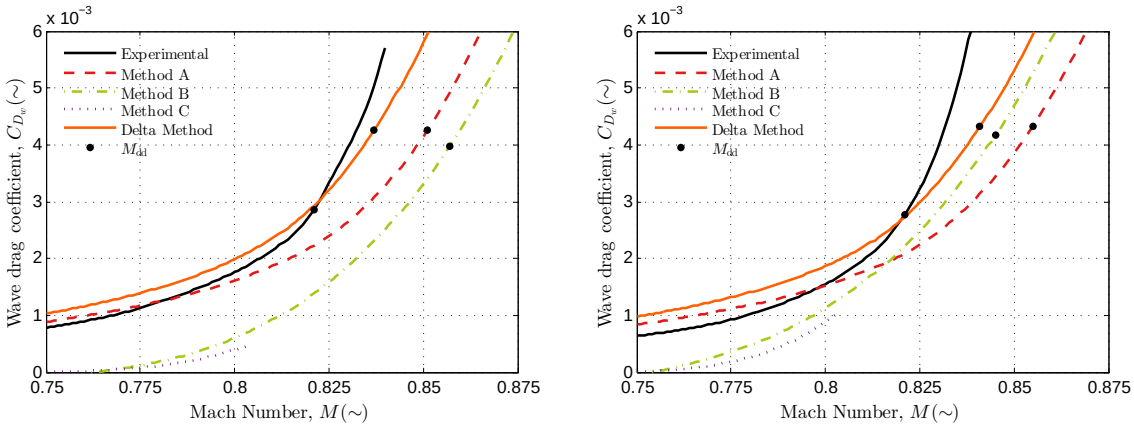

(a) $C_L = 0.2$

(b) $C_L = 0.3$

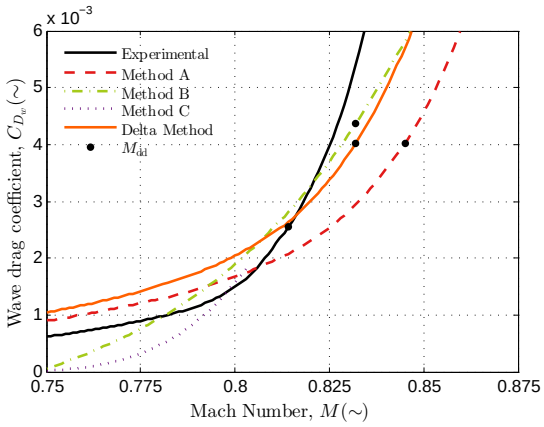

(c) $C_L = 0.4$

Figure 4.2: Experimental C_{D_w} of the Boeing 737-800 [17] compared to estimated data

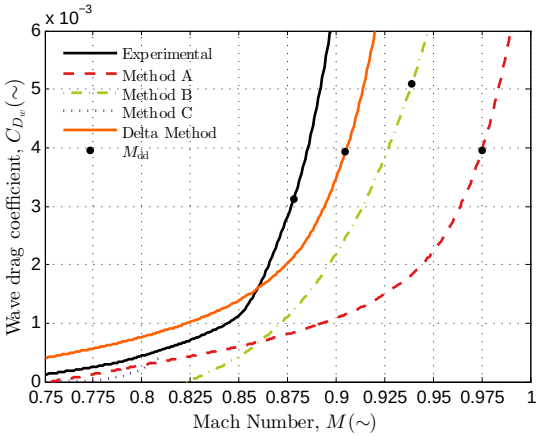

(a) $C_L = 0.3$

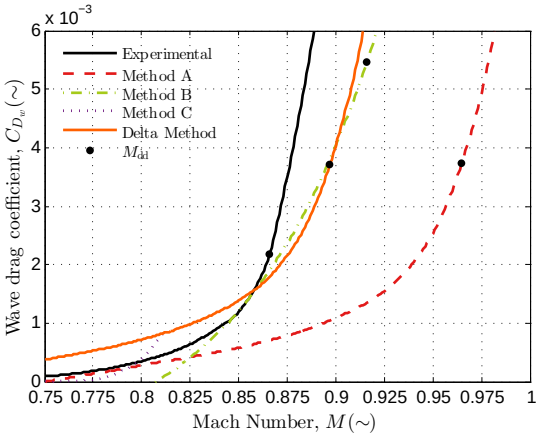

(b) $C_L = 0.4$

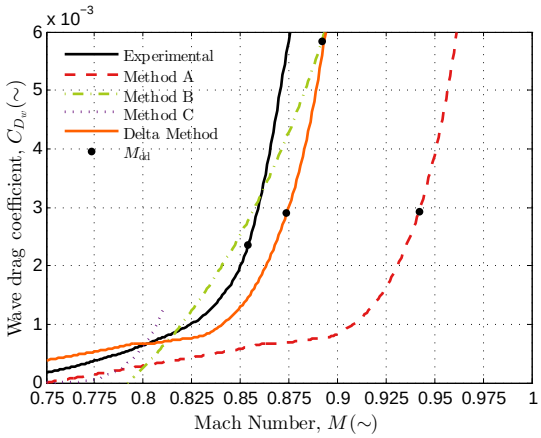

(c) $C_L = 0.5$

Figure 4.3: Experimental C_{D_w} of the Boeing 747-100 [17] compared to estimated data

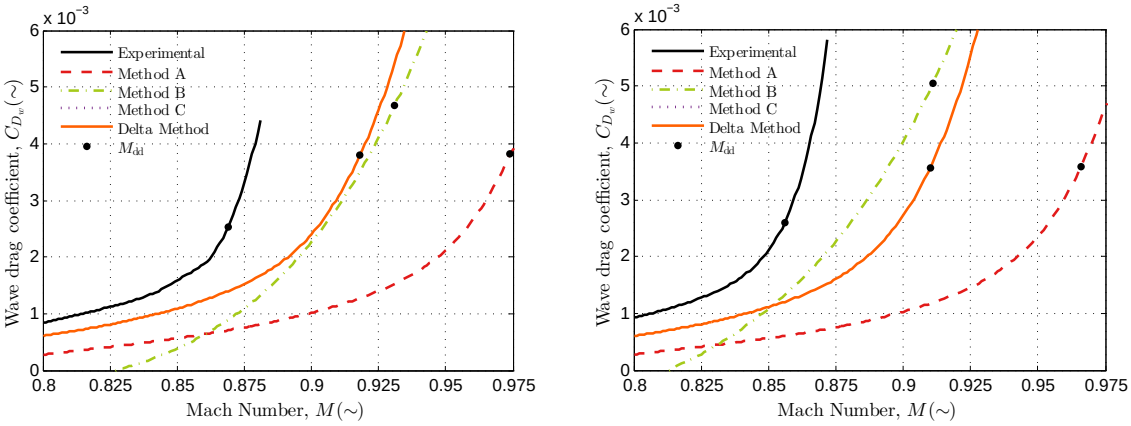

(a) $C_L = 0.3$

(b) $C_L = 0.4$

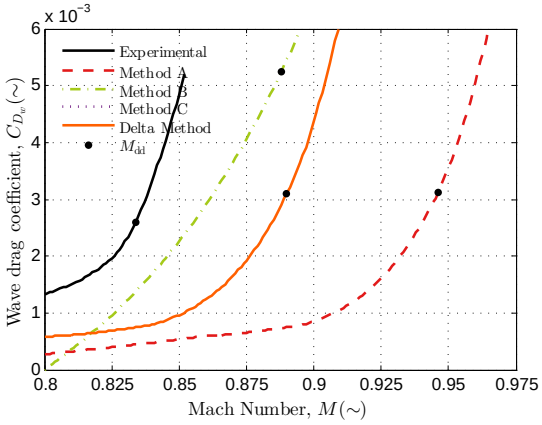

(c) $C_L = 0.5$

Figure 4.4: Experimental C_{D_w} of the McDonnell Douglas DC-10-30 [17] compared to estimated data

- The absolute error $\left|e_{C_{D_w}}\right| = \left|\Delta C_{D_{w\text{exp}}} - \Delta C_{D_{w\text{est}}}\right|$, where ΔC_D is measured at $M = 0.8$, is used to measure how close the methods predict the wave drag coefficient at a Mach number close to M_{cruise}. A graphical explanation is also shown in Figure 4.5 and results are shown in Figure 4.8.

- The root mean squared error (RMSE) is used to see how close is the prediction to the experimental data along the transonic range, or at least along the Mach number range predicted by each procedure. Results are shown in Figure 4.6.

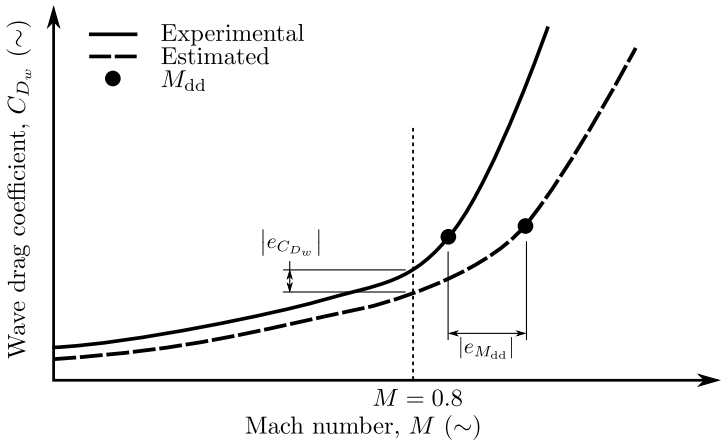

Figure 4.5: Error estimation

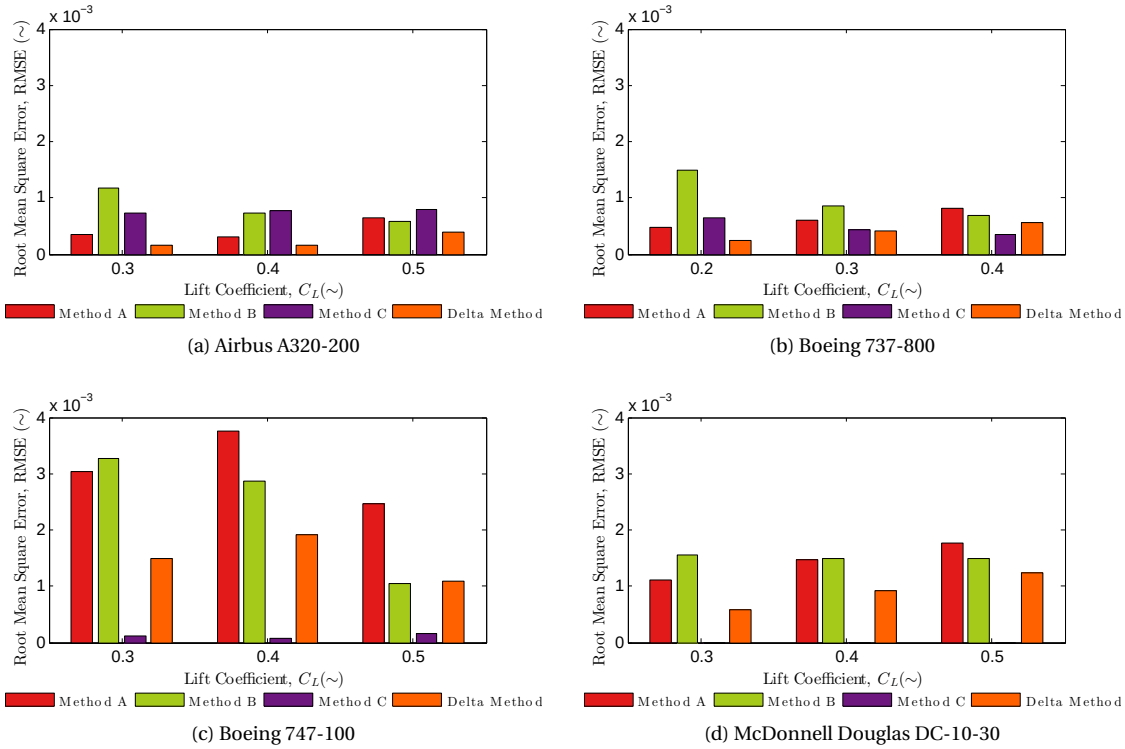

(a) Airbus A320-200

(b) Boeing 737-800

(c) Boeing 747-100

(d) McDonnell Douglas DC-10-30

Figure 4.6: Root Mean Square Error

The amount of information included in each method, as shown in Table 2.1, the data represented in Figures 4.1 to 4.4, as well as the information shown in Figures 4.6 to 4.8 lead to several observations described below.

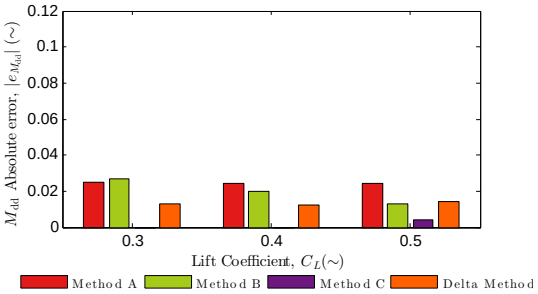

(a) Airbus A320-200

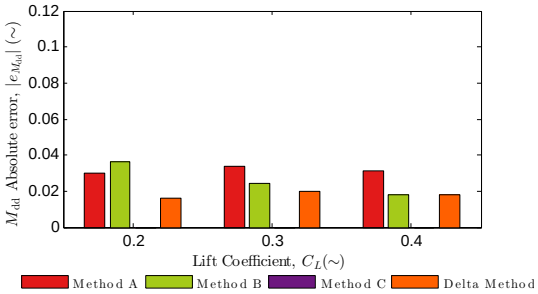

(b) Boeing 737-800

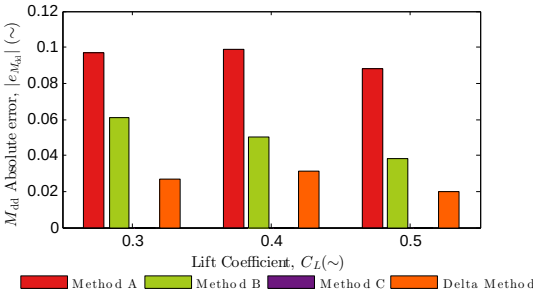

(c) Boeing 747-100

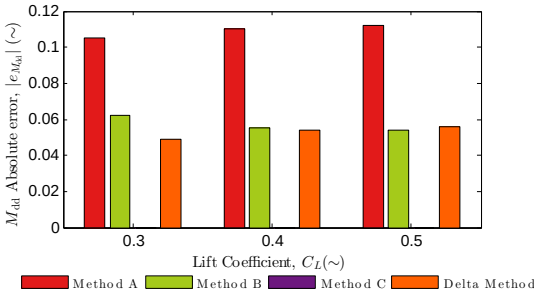

(d) McDonnell Douglas DC-10-30

Figure 4.7: M_{dd} prediction absolute error, $\left|e_{M_{\text{dd}}}\right| = \left|M_{dd_{\text{exp}}} - M_{dd_{\text{est}}}\right|$

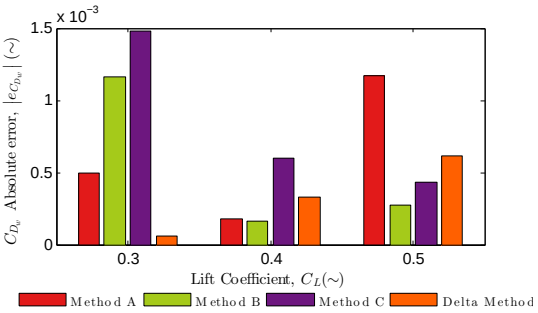

(a) Airbus A320-200

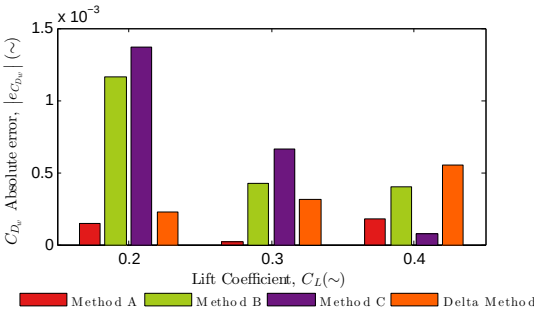

(b) Boeing 737-800

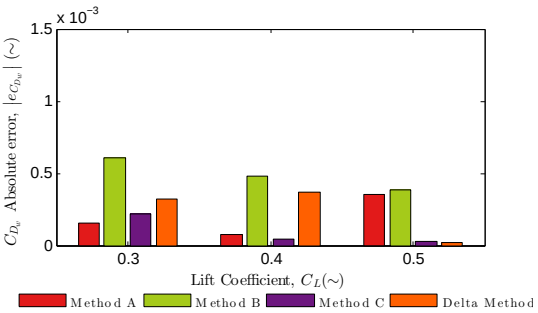

(c) Boeing 747-100

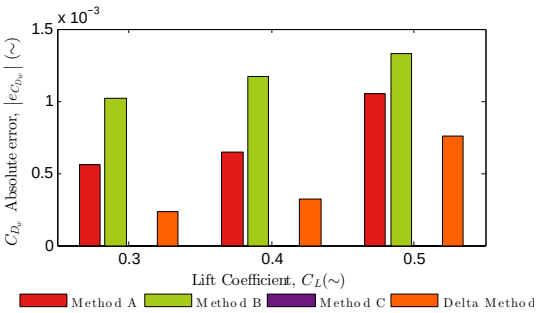

(d) McDonnell Douglas DC-10-30

Figure 4.8: C_{D_w} at $M = 0.8$ prediction absolute error $\left|e_{C_{D_w}}\right| = \left|C_{D_{w_{\text{exp}}}} - C_{D_{w_{\text{est}}}}\right|$

4.3.1. PROPOSED METHOD A - DISCUSSION

During the analysis, the proposed method A showed a couple of interesting aspects. Firstly, Figures 4.6a and 4.6b show that for the Airbus A320-200 and the Boeing 737-800 the estimations of wave drag coefficient using method A have a definitively lower RMSE than that of the long-range test cases of Figures 4.6c and 4.6d. It is also known from Table 3.1 that the short- to medium-range aircraft have wings with higher thickness to chord ratio, higher aspect ratio and lower sweep than those of the two test cases representing long-range aircraft. This corresponds, to some extent, with what is mentioned in Reference [2], which states that a better equivalence between a two- and a three-dimensional flow can be expected when analyzing wings of moderate sweep and high aspect ratio.

Secondly, it is also possible to see in Figure 4.7 that the error regarding the estimation of the drag divergence Mach number, $|e_{M_{\text{dd}}}|$, remains constant for each aircraft at different lift coefficients. This is a good indication of the method capabilities to represent the variation of the drag divergence Mach number as function of the lift coefficient. Likewise, the higher error of the Boeing 747-100 and McDonnell Douglas DC-10-30 can be related to the the fact that these aircraft are equipped with peaky airfoils, instead of supercritical airfoils. It is known from Reference [31] that supercritical airfoils are able to develop higher lift coefficients at higher drag divergence Mach numbers compared to peaky airfoils.

Thirdly, this method exhibits good capabilities estimating the drag creep. A feature obtained from the Delta method. This is especially true for the estimations of the Airbus A320-200 and the Boeing 737-800 of Figures 4.1 and 4.2, respectively. In these two cases the estimation of the drag creep added to the the good estimation of the drag divergence Mach number lead to a very good general agreement between the estimated and the experimental data. This also leads to the low RSME already mentioned. Drag creep is also present in the estimations of the Boeing 747-100 and the McDonnell Douglas DC-10-30.

Finally, the lower thickness to chord ratio of the McDonnell Douglas can be the reason why Method A, and also the other methods, tend to estimate values of drag divergence Mach number higher than the experimental value, as seen in Figures 4.4 and 4.7d.

4.3.2. PROPOSED METHOD B - DISCUSSION

During the analysis using the test cases described in Section 3.1, the proposed method B exhibited relatively good capabilities to estimate the drag divergence Mach number. Three important remarks can be made regarding the performance of this method. Firstly, the slight variations in the error of the drag divergence Mach number estimations, $|e_{M_{\text{dd}}}|$, are not necessarily bad since the error tends to decrease when increasing the lift coefficient. Typically, it is at high lift coefficients that the drag divergence Mach number becomes lower and more critical to the design by limiting more the performance of the aircraft.

Secondly, the fact that Equation 2.5 proposed by Torenbeek only considers supercritical airfoils [1] can be the reason why this method predicts higher drag divergence Mach number for the two long-range aircraft equipped with peaky airfoils, as shown in Figures 4.7c and 4.7d. Similarly, the slightly higher wing sweep and lower aspect ratio of the long-range aircraft can also induce errors in the estimation of the drag divergence Mach number. This is related to the lesser degree of equivalence usually expected between two- and three-dimensional flows [2] for higher wing sweep and lower aspect ratio.

Last but not least, the higher RMSE and absolute error of the estimation of the wave drag coefficient at a Mach number of 0.8, $|e_{C_{D_w}}|$, corresponds to the different way the drag builds up in the case of NACA 6-series airfoils compared to any advanced airfoil. The drag on a NACA 6-series airfoil builds up smoothly as observed in the estimations of this method, specially for sweeps between 0 and 30 degrees; whereas the drag rise is expected to be stronger for the same kind of wing due to the high aspect ratios [15]. The effect of the aspect ratio, however, is not strong enough to predict the more sudden drag rise typical of advanced airfoils. The reason behind this is the source of such drag build-up. In the case of the NACA 6-series airfoils or natural laminar flow airfoils, they are designed to maximize the critical Mach number [32]. As a consequence, they produce a significant amount of wave drag whenever they are exposed to Mach numbers beyond the critical Mach number. This is due to the formation of strong shock waves on the wing surface in combination with the separation at the shock foot [26]. In contrast, the design philosophy of the peaky and supercritical airfoils is to increase the interval between the critical Mach number and the drag divergence Mach number [3]. As a consequence, these airfoils are able to maintain a low level of drag beyond the critical Mach number. To achieve this, advanced airfoils have some specific properties. In the case of the peaky airfoils they have a sharp suction peak and high adverse pressure gradient in the subsonic pressure distribution. The significant amount of isentropic recompression can lead to shock-free airfoils or airfoils with a weak normal shock wave terminating the supersonic domain [26]. Similarly, in a supercritical airfoil the supersonic flow is closer to the

surface, it has lower local supersonic Mach numbers and the shock wave is weaker [23].

4.3.3. PROPOSED METHOD C - DISCUSSION

During the analysis, the proposed method C showed some limitations concerning its range of applicability. This became evident for the first time when analyzing the McDonnell Douglas DC-10-30. Due to the low average thickness to chord ratio of the wings of this aircraft, this method is not able to estimate any wave drag for such configuration as shown in Figure 4.4. The second limitation is related to the Mach number range along which the method is able to perform any estimation. From all the cases analyzed, the method was able to predict the drag divergence Mach number only on one situation; the Airbus A320-200 with a lift coefficient of 0.5 shown in Figure 4.1c. As a result, there is no information concerning the error of the estimation of the drag divergence Mach number, $\left|e_{M_{\text{dd}}}\right|$, in Figure 4.7.

The inability of this method to estimate the drag divergence Mach number leads to another issue. It was not possible to implement the correction from the two-dimensional Mach number to the three-dimensional Mach number as described in Section 2.3. As shown in Equation 2.9, this correction involves obtaining the two-dimensional drag divergence Mach number defined by the two-dimensional boundary $\partial c_d/\partial M$. This requirement worsens the situation even more since, as shown in Equation 2.10, the value of $\partial c_d/\partial M$ is usually higher than that of $\partial C_D/\partial M$, which means that an even longer Mach number range would be needed to reach the higher two-dimensional boundary.

For the Airbus A320-200, the Boeing 737-800 and the 747-100 it was possible to implement the method without the correction of Equation 2.9. As a result some effects can be observed. Firstly, the method does not estimate any drag creep but instead an oscillation similar to the one observed in Figure 2.5. The absence of drag creep in the estimations is directly linked to the absence of drag creep in the experimental data on which this method is based; especially the data regarding the airfoils with a thickness to chord ratio of 0.10 and 0.14 of References [21, 22]. The absence of drag creep in these particular airfoils is the result of a very extensive test campaign during the 1970's, in which reducing drag creep and other effects received an important amount of attention [23].

The absence of drag creep in the estimated data leads to the relatively high RMSE of the Airbus A320-200 and the Boeing 737-800 of Figures 4.6a and 4.6b, respectively. However, despite the high RMSE, the two short- to medium-range aircraft equipped with supercritical airfoils exhibit certain degree of correspondence between the experimental and estimated data. This is especially true at low lift coefficients, where the estimations seem to run parallel to the experimental data, as seen in Figures 4.1 and 4.2.

The low RMSE of the estimations of the Boeing 747-100 using this method, might be related to the drag creep development of this aircraft. As shown in Figures 3.1a to 3.1c, the drag creep of the Boeing 747-100 is lower compared to the short- to medium-range aircraft. However, the drag rise behavior of the estimations differs considerably from the experimental data. It might be possible that the early drag rise observed in the estimated data of the Boeing 747-100, as shown in Figure 4.3, is due to the absence of correction in the Mach number. This differences might be also more noticeable for the Boeing 747-100 due to its higher sweep angle compared to the Airbus and the other Boeing.

4.3.4. DELTA METHOD - DISCUSSION

From all the methods described in the state of the art, the Delta method includes the highest number of variables. Likewise, it is the only method found in the literature that is originally designed to predict the wave drag development for advanced airfoils in the transonic regime. Figures 4.1 to 4.4 show that the method is good at estimating drag creep as well as the drag divergence Mach number. Additionally, the fact that the Delta method is based on experimental data from advanced airfoils leads to estimations that exhibit drag rise characteristics very close to those of advanced airfoils. The low RMSE values of Figure 4.6 are also proof of the accuracy of the method. Since method A is based on the Delta method, they have some similarities. Like in the method A, Figure 4.7 shows that the error in estimating the drag divergence Mach number, $\left|e_{M_{\text{dd}}}\right|$, remains constant when varying the different lift coefficient of each aircraft. This is, as mentioned earlier, a demonstration of the method capabilities to estimate the variation of the drag divergence Mach number as function of the lift coefficient.

In the case of the McDonnell Douglas DC-10-30 the Delta method also estimates a drag rise at a higher Mach number than the experimental value, as seen in Figure 4.4. According to Equation 1.2, and the information from the Table 3.1, this aircraft has the lowest average thickness to chord ratio from the four test cases. This might be the reason for the higher displacement of the estimations when compared to other aircraft. The Boeing 747-100 tends to have a similar behavior, but less severe.

4.4. COMPARISON WITH THE KORN-LOCK METHOD

From the analysis, it can be seen that the three proposed methods do not always exhibit a higher level of accuracy compared to the Delta method. The Delta method surpasses the level of accuracy of the three proposed methods, especially in the test cases with thicker airfoils. Although the Delta method does not include the highest number of design parameters compared to the proposed methods, it is based on experimental data of advanced airfoils. This leads to better estimation of the drag rise characteristics. The previous results and analysis show that, among the methods included in this document, the Delta method seems to be the most suitable technique to predict the wave in the conceptual design phase of conventional passenger aircraft.

Figures 4.9 and 4.10 show the comparison between the Korn-Lock method and the Delta method. A potential improvement of up to 22 counts can be observed in the case of the estimation of the wave drag coefficient at $M = 0.8$. Similarly, the improvement in the prediction of drag divergence Mach number goes up to about 0.04. The First case corresponds to the analysis of the Airbus A320-200, and the second to the Boeing 747-100. Both at low lift coefficients. In general, the improvement in the predictions obtained with the Delta method for the A320-200 and the Boeing 737-800 seems to be higher at lower lift coefficients. In the case of the more elusive DC-10-30 the improvement is lower but less sensitive to the lift coefficient.

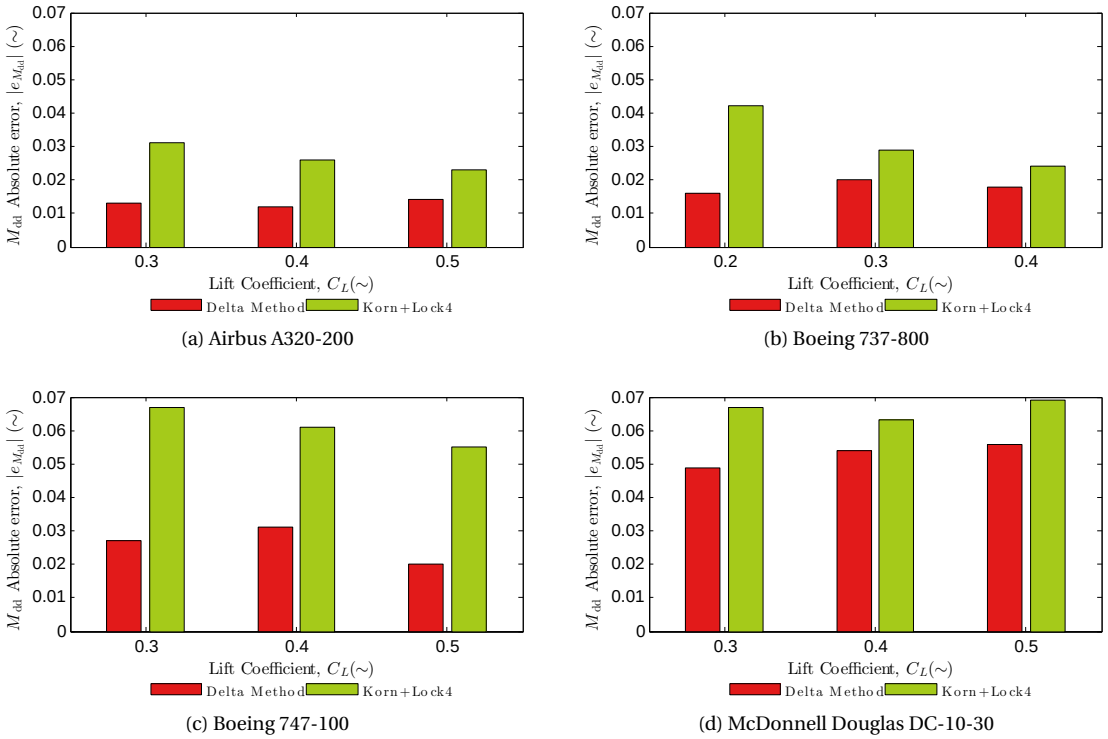

(a) Airbus A320-200

(b) Boeing 737-800

(c) Boeing 747-100

(d) McDonnell Douglas DC-10-30

Figure 4.9: M_{dd} prediction absolute error, $\left|e_{M_{\text{dd}}}\right| = \left|M_{dd_{\text{exp}}} - M_{dd_{\text{est}}}\right|$

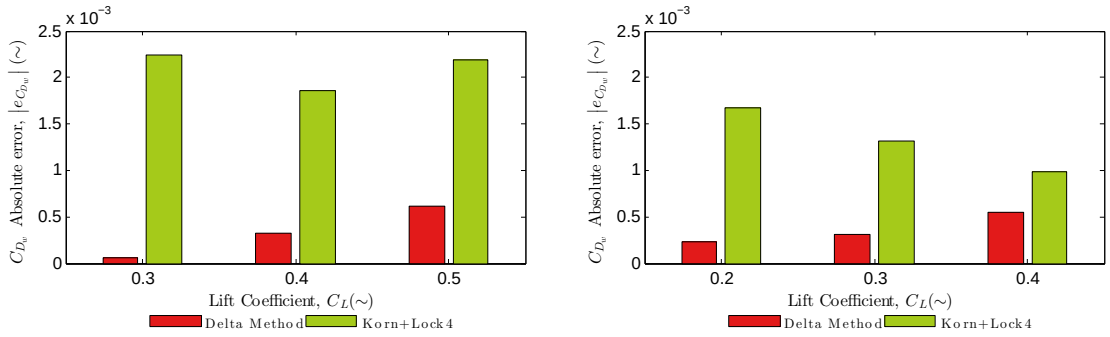

(a) Airbus A320-200

(b) Boeing 737-800

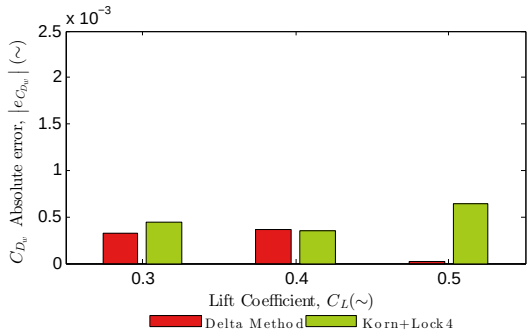

(c) Boeing 747-100

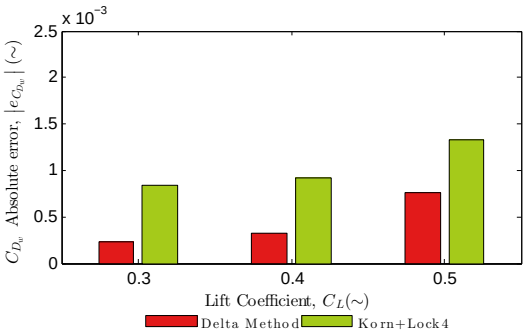

(d) McDonnell Douglas DC-10-30

Figure 4.10: C_{D_w} at $M = 0.8$ prediction absolute error $\left|e_{C_{D_w}}\right| = \left|C_{D_{w_{\text{exp}}}} - C_{D_{w_{\text{est}}}}\right|$

5

CONCLUSIONS AND RECOMMENDATIONS

5.1. CONCLUSIONS

The objective of this project is to improve the wave drag prediction of fixed wing aircraft at low transonic conditions in the conceptual design phase. A new module of the Initiator was developed to answer the research question: *is it possible to improve the wave drag prediction methods by including more design variables, or by adapting them to the current technologies and aircraft specifications?*.

To answer the previous question and meet the objective of the project three methods were proposed. These methods are based on existent techniques and include more design variables than the original versions. Four well documented test cases were used to validate the proposed methods. The four cases were conventional aircraft configurations and represented short- to medium-range and long-range aircraft. An accuracy analysis was conducted to evaluate the performance of the methods. The accuracy analysis included the most promising state of the art technique as reference.

Although wing design parameters are the driving factors of the wave drag estimation, the fuselage was also considered in all the methods proposed. The procedure used to estimate the fuselage wave drag allow one to include more parts of the aircraft in the analysis.

The first proposed method was an attempt to include more design parameters as part of the equivalence between a two and a three-dimensional flow. The results of these approach showed a drag rise behavior displaced to a higher Mach number than that of the experimental data. The displacement was bigger in aircraft having lower aspect ratio and higher wing sweep. This can be associated to the lesser equivalence usually expected under these circumstances.

The second proposed method was an attempt to use a very well known technique based on outdated airfoils and adapt it to a more recent and advanced airfoil design. However, it was observed that the differences in the design approach of an airfoil play an important role in the drag rise characteristics of a wing. As a result the method fails to predict the wave drag of the test cases considered.

The last proposed method was an attempt to create a set of correlations based entirely in experimental data from advanced airfoils. Additionally, the same framework used in the first method to transform the results from a two-dimensional to a three-dimensional flow was used also as an attempt to include more design parameters in the procedure. The restricted amount of experimental data used in the formulation of the correlations resulted, however, in a procedure with a very limited application range.

One of the methods from the state of the art was included in the analysis of the proposed methods. The procedure, known as Delta method, exhibited the most satisfactory results in the initial study. It also produced the most satisfactory results when it was validated using the test cases representing conventional aircraft. When compared to the Korn-Lock method (procedure originally used in the Initiator) the Delta method showed an improvement in the prediction of the wave drag coefficient at a specific Mach number of up to 22 counts. The estimation of the drag divergence Mach number was also improved by up to 0.04.

Despite the improvements just mentioned, the opportunities are still open to evaluate more combinations or possibilities that can lead to even more accurate wave drag estimation procedures.

5.2. RECOMMENDATIONS

After analyzing the methods discussed in this document some recommendations can be given regarding the inclusion of more experimental data, the implementation of additional external tools, the analysis of more phenomena that occur at transonic speeds, and the analysis of non-conventional configurations.

Including more experimental data regarding the drag development of supercritical airfoils would lead to a significant improvement of the proposed method C. First of all, including experimental data at zero-lift would allow one to separate the analysis into zero-lift and lift dependent drag coefficient. As a result, it would be possible to obtain a specific set of correlations, including different design parameters, to each condition. This is important since the impact of each design parameter on the zero-lift coefficient might be different from the impact on the lift dependent drag coefficient. The different correlations proposed by McDevitt are an example of this. Similarly, including additional information of the geometry of the airfoil, such as the camber, can also improve the accuracy of the procedure. For example, it is known that different airfoil shapes can influence the dependency of the drag divergence Mach number to parameters such as the lift coefficient [26].

The implementation of an external tool specialized in the geometrical analysis of tree-dimensional surfaces can help to improve the area distribution estimation. This is especially valid if the geometry of new additional surfaces, such as the pylons or the wing-body fairing, is generated by future versions of the Initiator. Obtaining the intersections between the surfaces or calculating the cross sectional area is a task at which MATLAB is not specially efficient. This improvement can save time in the execution of the module. Similarly, in the case of low aspect ratio configurations, it would be possible to include the area distribution of the whole aircraft, including the wings, as part of the analysis. This can be done by comparing the area distribution of an aircraft to that of an optimal body. The comparison of these two area distributions is based on the fact that two bodies with the same cross sectional area have the same drag rise characteristics, as described by Whitcomb in Reference [33]. It is not possible to transform the area distribution into a wave drag coefficient for Mach numbers lower than one. However, this comparison can be used as reference for locating different surfaces that do not contribute to the maximum cross sectional area, which is the parameter used in the methods described in this document.

The methods analyzed in this document rely on the very few variables known during the conceptual design phase. As a result it is difficult to separate the different phenomena that occur during flight. A clear example is the calculation of the wave drag due to lift. Methods such as the one proposed by McDevitt allow the designer to estimate the total drag due to lift. Similarly, the Delta method allows the designer to estimate the increment in pressure drag, which includes the contribution of separation, lift dependent compressibility drag, span-wise flow, among others. To tackle this, only the variation respect to a initial value along the low transonic range was considered. However, trying to estimate separately the contribution from each phenomenon on the drag coefficient, might result in a more accurate solution. Likewise, including an estimation of the pressure distribution around the airfoils can also help to improve the calculation of the rooftop length. This would lead to a better estimation of the effective sweep, and as a consequence a more accurate transformation from two-dimensional flow to three-dimensional flow when using the framework of Reference [2]. Similarly, the methods analyzed in this document commonly assume that values such as the friction drag do not change along the transonic range. Implementing a method that estimates the variation of such value can help to improve the overall accuracy of the estimation of the total drag coefficient.

Concerning the analysis of non-conventional aircraft configurations, there was not any well documented test case that could be used in this project. As a result the methods proposed in this thesis still need to be validated for non-conventional configurations. Few suggestions were mentioned in Section 2.4. However, in the case of aircraft equipped with forward swept wings one has to be cautious with the methods and the corrections from two- to three-dimensional flow discussed in this document, since they are based mainly on conventional aft swept wings. The differences in the interaction between the wing and body of a forward swept wing, compared to an aft swept wing, can lead to different pressure distributions. As a result the position of the shock waves respect to the chord can change, and consequently the effective angles.

II

Code Documentation

6

INTRODUCTION

This Part describes the analysis module developed to locate all the functions needed to estimate the wave drag coefficient of an aircraft during the conceptual design. Chapter 7 describes the module structure and the methods needed to operate it. Chapter 8 explains how to operate the module, including also a description of the settings, outputs warnings and dependencies.

6.1. BACKGROUND

The methods implemented in the module allow the designer to estimate the wave drag of an aircraft flying at the low transonic regime. Since these methods are based on experimental data, its reliability is higher in conventional configurations. The reliability of the methods in non-conventional configurations has still to be tested. The module is part of the Initiator initially developed by Elmendorp and described in Reference [9].

6.2. INITIATOR

As mentioned in Section 1.3.1, the Initiator is an aircraft design tool oriented to the the design of conventional and non conventional configurations based on a set of top-level requirements. It is focused on conventional tube and wing aircraft, canard, three-surface, prandtl and blended-wing-body aircraft. It has been developed in a modular way using object-oriented programming [9].

Figure 6.1 shows the N^2 chart of the modules. Four types of modules are defined: Sizing, analysis design and work flow modules. Sizing modules perform the preliminary sizing and are those enclosed by the first black rectangle in Figure 6.1. The design then is passed to the analysis modules, which performs calculations concerning the weight, aerodynamic and others; and also design modules which calculate specific parts such as the cabin or the control surfaces. The analysis and designed modules are enclosed by the second black rectangle in Figure 6.1. The work-flow modules facilitate the Initiator to, for example, converge to a consistent design or read inputs and generate outputs [9]. To be able to converge, the Initiator has two loops represented in Figure 6.1 by the red boxes. The inner loop guarantees that the weight and aerodynamic loads converge. The outer loop ensures that the wing loading and weights converge [9].

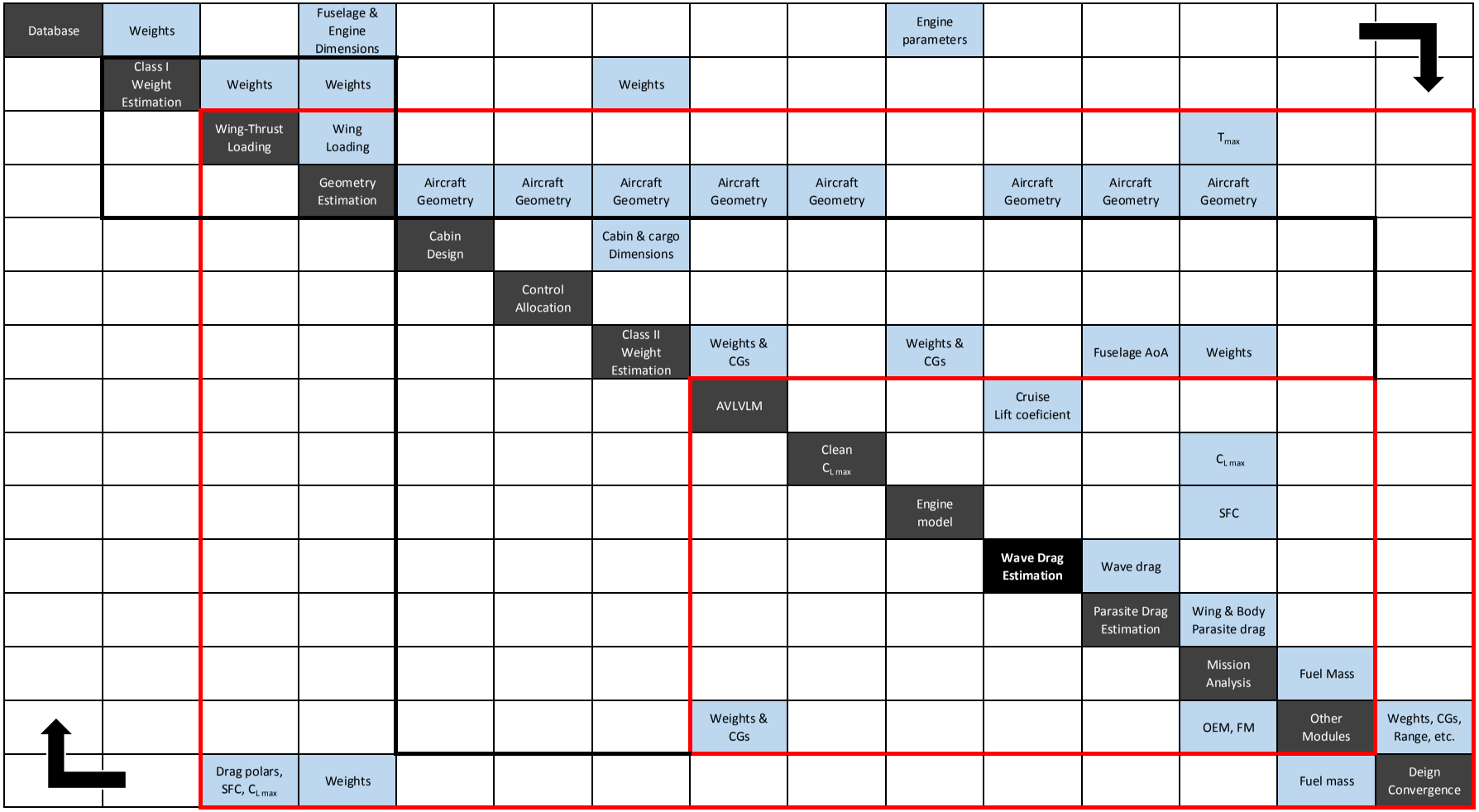

Figure 6.1: N^2 diagram of the Initiator (Adapted from Reference [9])

7

MODULE STRUCTURE

This Chapter describes the module designed to allocate the methods used to estimate the wave drag of an aircraft. Section 7.1 includes a module overview and the description of the main functions of the module. Section 7.2 describes the dependencies of the module and its operation.

7.1. MODULE OVERVIEW

The functions necessary to estimate the wave drag coefficient under transonic conditions are located into an analysis module. This module is called `WaveDragEstimation` and is a subclass of the *AnalysisModule* class. Similar to the other modules of the current version of the Initiator, this module was developed in MATLAB. Likewise, it uses the object-oriented programming functionality.

The module overview is shown in Figure 7.1, which represents the main file *run.m*. It is possible to identify four main actions in the activity diagram, namely: Calculate wing wave drag, calculate fuselage wave drag, create output variables, and create plots. The calculation of the wing wave drag varies according to the type of aircraft including those configurations that have a main wing, and the Prantl plane which has a box wing.

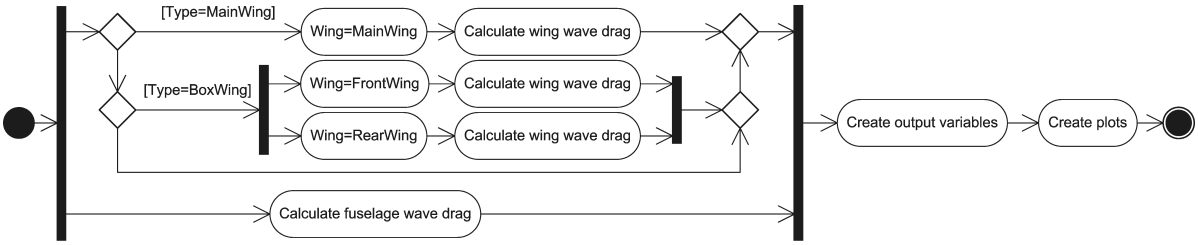

Figure 7.1: Activity diagram of *run.m*

The actions *calculate wing wave drag* and *calculate fuselage wave drag* correspond to two of the main methods of the module `WaveDragEstimation`. Namely the `Wing WaveDragTransonic` method and the `Fuselage WaveDragTransonic` method, respectively.

7.1.1. FUNCTION WINGWAVEDRAG

The function `WingWaveDragTransonic` is shown in Figure 7.2. The following cases can be identified:

- *Delta method* which refers to the method explained in the Section 1.3.2.
- *Delta method + ESDU* which refers to the first method proposed in this document, known as Method A, and explained in Section 2.1.
- *McDevitt* which refers to the method explained in Section 1.3.3.
- *McDevitt+Torenbeek* which refers to Method B; the second method proposed in this document and explained in Section 2.2.

- *Korn + Lock* which refers to the method explained in Section 1.3.1.
- *SCCorrelations* which refers to the third method proposed in this document, known as Method C, and explained in Section 2.3.

The case is chosen according to the module settings variable `WaveDragEstMethod`. The first four methods are arranged in two main groups in which the wave drag is calculated separately for non-lifting and lifting conditions and then summed. In contrast, the last two methods estimate the wave drag as a whole. All the methods include at some point a transformation from two-dimensional to three-dimensional flow.

METHODS NEEDED FOR CALCULATING WING WAVE DRAG

The activity diagram shown in Figure 7.2 includes few activities that were implemented as methods of the module `WaveDragEstimation` namely:

Torenbeek M_{dd} Calculating M_{dd} according to Torenbeek's equation was implemented as method. This function is able to obtain both two-dimensional and three-dimensional drag divergence Mach number using Korn's equation and Torenbeek's Equation 2.5, respectively.

Find M_{dd} Calculating the drag divergence Mach number for a given function $C_D(M_\infty)$ was also implemented as a method. If the data set of the wave drag coefficient is given along a Mach number range, this function is able to find M_{dd} using any of the two definitions given in Section 1.2, namely: ΔC_D or $\partial C_D/\partial M$. The boundary is specified in the settings of the module using the fields `DragRiseBoundaryMethod` and `DragRiseBoundaryValue`.

Airfoil type check The method `AirfoilTypeCheck` was implemented to identify if supercritical airfoils are being used or not. To accomplish this the method reads first the aircraft configuration parameter looking for a field `SupercriticalAirfoils`. If the field does not exist, the function reads the name of the airfoils looking for strings such as 'SC' or 'N6'. If there are not such strings, the function last resource is to detect some specific geometrical parameters of a supercritical airfoil. Based on all this, it is able to determine the kind of airfoil. The geometrical parameters are also part of the settings in the variable `SCAirfoilGeometry` of the vector type. The vector `SCAirfoilGeometry` contains the stations $(x/c)_1$, $(x/c)_2$, and $(x/c)_3$ as defined in Figure 7.3. If the lower surface of the airfoil meets the following three conditions, the airfoil is assumed to be supercritical:

- $\left.\frac{d^2z}{dx^2}\right|_{(x/c)_1} < 0$, indicating negative curvature in the aft lower surface.
- $\left.\frac{d^2z}{dx^2}\right|_{(x/c)_2} \geq 0$, indicateing positive curvature in the forward lower surface.
- $\left.\frac{dz}{dx}\right|_{(x/c)_3} < 0$, indicating negative slope in teh aft lower surface.

ESDU correlations The method `ESDUCorrelations` was implemented to be used as part of the methods A and C described in Sections 2.1 and 2.3, respectively. It calculates the three-dimensional equivalent of a specific variable according to Equations 2.1, 2.7, 2.8, 2.9, and 2.10 from Reference [2].

7.1.2. FUNCTION FUSELAGEWAVEDRAG

The function `FuselageWaveDragTransonic` is shown in Figure 7.4. It is entirely based on the method proposed by Feaguin and Morrison in Reference [7] and includes the calculation of the cross sectional area distribution of all the bodies and surfaces, except the wings. These calculations have been defined as methods of the `WaveDragEstimation` module.

METHODS NEEDED FOR CALCULATING FUSELAGE WAVE DRAG

The activity diagram shown in Figure 7.4 includes several activities that were implemented as methods of the module `WingWaveDragTransonic`. These activities are described below.

Area distribution of a existing part As explained in Section 3.2, the process to obtain the cross sectional area distribution of the parts previously defined in the Initiator always involves dividing the geometrical three dimensional coordinates into left and right. Then some intersections should be obtained according to the location of the part. If the location of the part includes also the possibility of being at center or at left or right, extra procedures should be considered, in the case of the engine the outer part of the nacelle is separated from the inner part. The number of sections into which each part and then the whole aircraft is divided is defined by the setting `AreaDistributionSections`.

Area distribution of the pylon estimation As explained in Section 3.2.2, the method `ADPylonEst` estimates the area distribution based on the geometry of the nacelle, its position respect to the wing or fuselage, and the geometry of an airfoil specified in the module settings by the setting `PylonEstimationAirfoil`. The maximum pylon chord respect to the nacelle length is set with the setting `EngineLengthPylonMaxLength`. In the case of fuselage mounted engines, the variable m_{pylon} of Equation 3.9 is set with the setting `PylonTanLambda`. Similarly, the setting *PylonIntoFuselage* is used to calculate $y_{\text{le}_{@\text{fuselage}}}$.

Area distribution of the wing-body fairing As explained in Section 3.2.2, the method `ADWingRootEst` uses the information given in References [28, 29] and the inputs given in the setting `FairingProportions` to estimate the contribution to the cross sectional area distribution of the fuselage.

7.2. MODULE DEPENDENCIES

The variables just mentioned can be obtained by running the `AVLVLM` module. This module is able to calculate the drag polar and the design lift coefficient [9, 34]. In order to do so, the same module also needs the other geometrical variables necessary to perform the wave drag estimation.

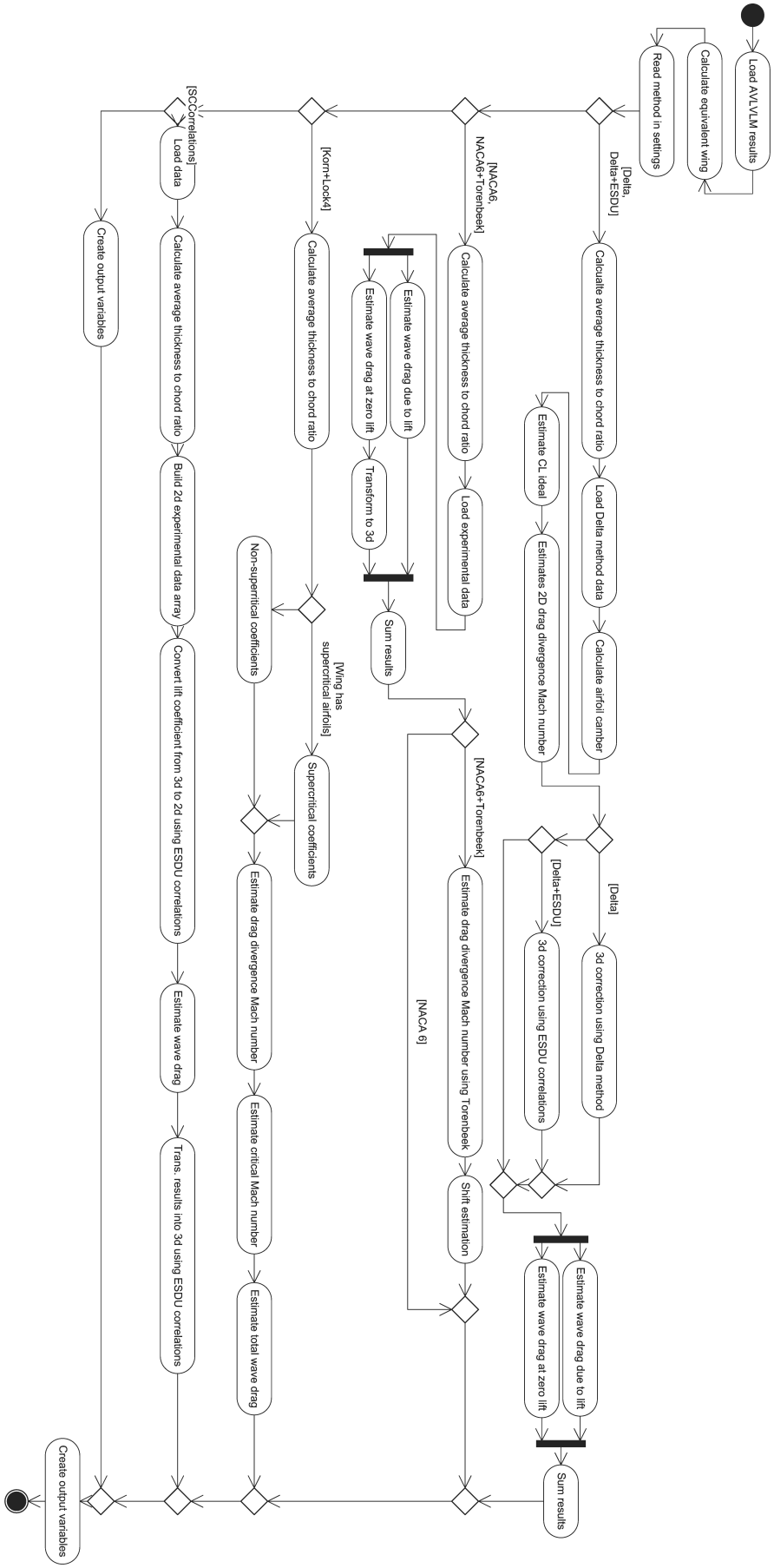

Figure 7.2: Activity diagram of `WingWaveDragTransonic`

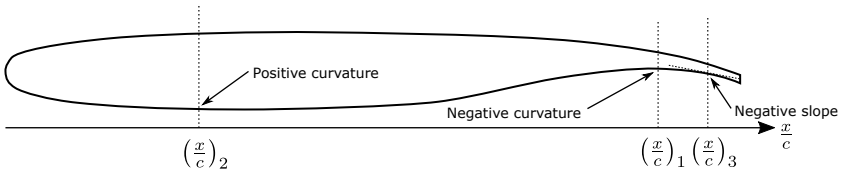

Figure 7.3: Supercritical airfoil detection

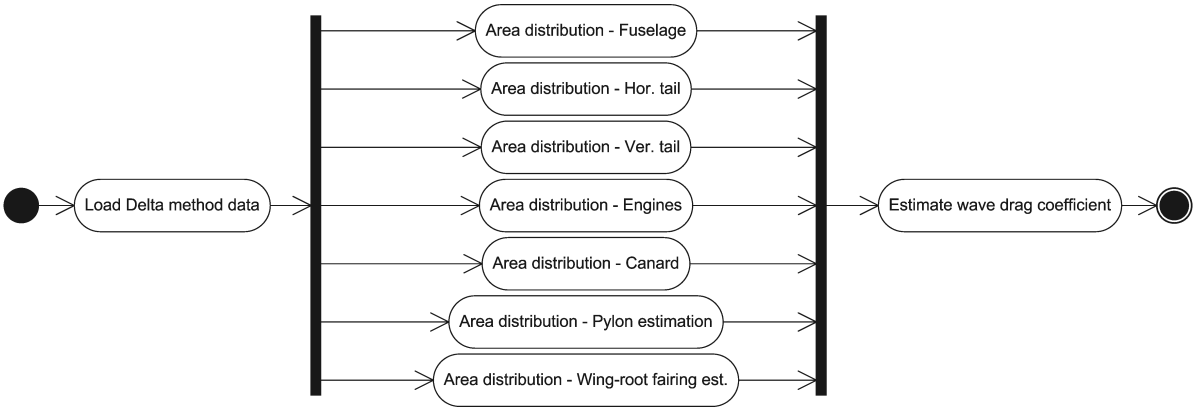

Figure 7.4: Activity diagram of `FuselageWaveDragTransonic`

8

USER MANUAL

This Chapter includes user manual and instructions to operate the module. Section 8.1 describes the procedure to run the module. Section 8.2 describes the different settings available. Section 8.3 describes the outputs of the module, including plots and variables. Finally, Section 8.4 describes the warning messages given by the module during its normal operation.

8.1. RUNNING THE MODULE

The module can be run by running the Initiator in MATLAB:

1. `Initiator;`
2. `C = InitiatorController('aircraft.xml');`
3. `C.runModule('WaveDragEstimation');`

The module can also be run in the interactive mode of the Initiator:

1. `Initiator -interactive aircraft.xml`
2. `run WaveDragEstimation`

8.1.1. RUN TIME

The current running time of the module is about 6 seconds for a common airliner such as the Airbus A320-200. This includes: the estimation of the area distribution, including the calculation of the intersection between the tail surfaces and the fuselage; and the estimation of the wave drag based on the experimental data from the Delta method.

8.2. SETTINGS

The method employed to estimate the wave drag of an aircraft can be set up in the file `settings.xml`. The same file allows the user to set other properties like the drag rise boundary defined in Section 1.2, and the estimated pylon profile described in Section 3.2.2, among others. All options are listed in Table 8.1.

8.3. OUTPUTS

The module `WaveDragEstimation` has two types of outputs. First, the variables that can be read by other modules; and second, the plots that can be used by the user of the software. Both of them are described below.

8.3.1. VARIABLES

Several variables are available as output of the module. All of them are saved into the property *Results* and are described below:

Table 8.1: Settings `WaveDragEstimation`

Name	Description	Expected Value
WaveDragEstMethodSC	Method for supercritical airfoils	Method from Table 8.2
WaveDragEstMethodNonSC	Method for non-supercritical airfoils	Method from Table 8.2
DragRiseBoundaryMethod	Drag rise boundary method	dCDdM, DeltaCDw
DragRiseBoundaryValue	Drag rise boundary	$\partial C_D/\partial M$, ΔC_D
PylonEstimationAirfoil	Pylon airfoil	Airfoil name
FairingProportions	Proportions of the estimated fairing	vector i.e.: $(4,8,4)$
AreaDistributionSections	Number of cross sections	Integer number
EngineLengthPylonMaxLength	Max. pylon length respect to engine	Number between 0 and 1
PylonTanLambda	Slope leading edge of pylon	Number between 0 and 1
PylonIntoFuselage	Fuselage radius occupied by pylon	Number between 0 and 1
TransonicMachRange	Transonic range	vector i.e.: M_{low}, M_{high}, npoints
SCAirfoilGeometry	x/c stations of Figure 7.3	vector x/c_1, x/c_2, x/c_3

Table 8.2: Wing wave drag prediction methods

Method names
Delta
Delta+ESDU
McDevitt
McDevitt+Torenbeek
Korn+Lock
SCCorrelations

- `Results.M` contains the Mach number transonic range defined by the setting `TransonicMachRange`. It is basically an equally spaced vector starting at M_{low}, and finishing at M_{high}.
- `Results.CDw_wing` contains the wave drag coefficient of the wing alone along the transonic range. It is also a vector with the same size of `Results.M`.
- `Results.CDw_fus` contains the wave drag coefficient of the fuselage including the tail, engine nacelles, canard (if any), pylons and wing-body fairing. The coefficient is expressed along the transonic range. This variable is also a vector with the same size of `Results.M`.
- `Results.TCDw` is the total wave drag coefficient of the aircraft along the transonic range. Similar to the previous variables, it is also a vector with the same size of `Results.M`.
- `Results.TCDw_cruise` is the wave drag coefficient at cruise Mach number. This is the variable used by the `ParasiteDragEstimation` module.
- `Results.Mdd` is the drag divergence Mach number obtained from the estimated curves according to the boundary established in the settings.

From all the output variables previously mentioned, only `Results.TCDw_cruise` is currently used by other modules. As mentioned before, this variable is included into the `ParasiteDragEstimation` module, which is called during the execution of the `MissionAnalysis` module. There, the drag polar is used to estimate the performance of the aircraft during different phases including cruise condition. Here the wave drag prediction plays an important role. In contrast, the other variables are available for future developments.

8.3.2. PLOTS

Three plots are generated by the module `WaveDragEstimation`. The plots are generated by running the `PlotTool`, or by exploring the folder **/Initiator/.plots/WaveDragEstimation* after running the module. The three plots are described below.

PLOT $C_{D_w} = f(M, C_L)$

The first plot generated by the module shows the estimated wave drag for the wing and the fuselage separately. A vertical line shows the estimated drag divergence Mach number as reference. Another vertical line shows the cruise Mach number. The intersection between the last one and the estimated total wave drag coefficient corresponds with the wave drag coefficient used by the `ParasiteDragEstimation` and the `MissionAnalysis` modules. An example of this plot is shown in Figure 8.1

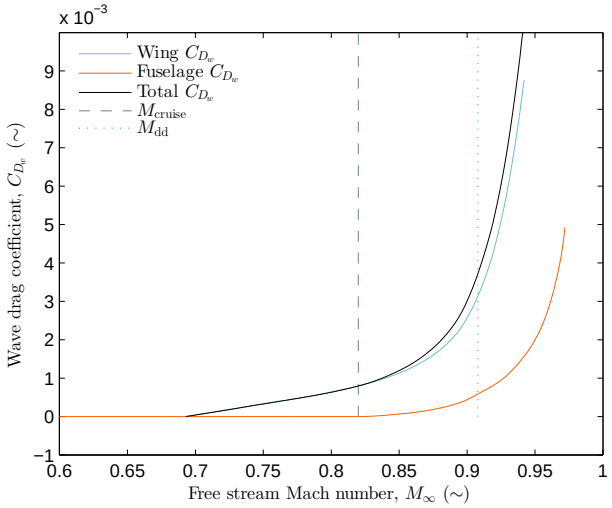

Figure 8.1: Module plot - Wave drag estimation

PLOT CROSS SECTIONAL AREA DISTRIBUTION

The second plot generated by the module shows the cross sectional area distribution as described in Section 3.2. As mentioned before this analysis is part of the procedure to estimate the fuselage wave drag coefficient. An example of this plot is shown in Figure 8.2.

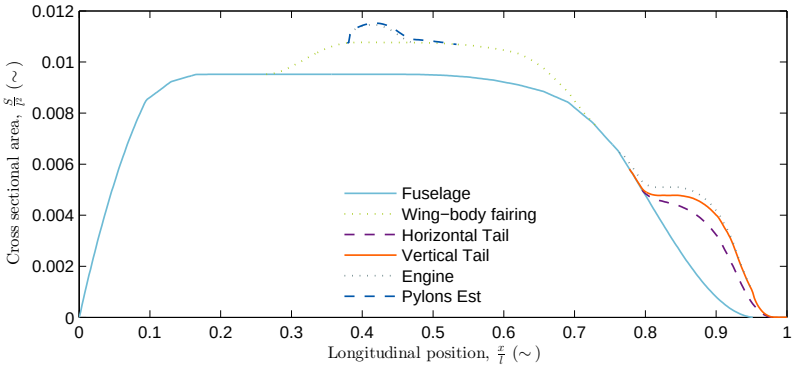

Figure 8.2: Module plot - Cross sectional area distribution

PLOT OF THE AIRCRAFT PARTS INCLUDED IN THE CROSS SECTIONAL AREA DISTRIBUTION

The third and last plot generated by the module shows the three-dimensional representation of the parts involved in the calculation of the cross sectional area distribution. The parts are represented after the intersections are calculated. As a visual aid, one of the warnings explained in Section 8.4 is linked to this graph by altering the colors of the surfaces in conflict. More details are given in the explanation of the specific warning. An example of this plot is shown in Figure 8.3.

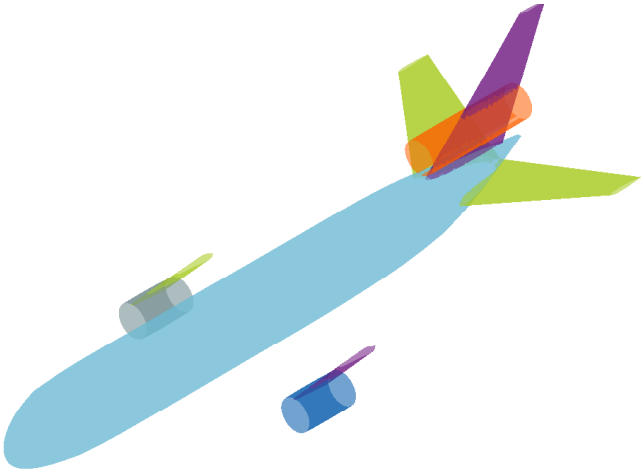

Figure 8.3: Module plot - Parts included in the cross sectional area distribution

8.4. ERRORS OR WARNINGS

8.4.1. UNSOLVED INTERSECTIONS

The method `CalculateIntersections` can generate a warning if the intersection between two surfaces is not clearly determined. Under certain conditions the method `SurfaceIntersection` cannot determine the intersection between two surfaces. In this case the area distribution then is calculated without considering the intersection of two surfaces. The three-dimensional representation of the surfaces described in Section 8.3.2 automatically shows the conflicted surface in red. Likewise, the warning described below is shown in the command line:

`Intersection not calculated between:` *`Surface A`* `and` *`Surface B`*

Unsolved intersections can be solved with slight changes in the positioning of the surfaces.

8.4.2. UNKNOWN DRAG RISE BOUNDARY

The method `FindMdd` can generate two different warnings. The first warning make reference to the settings and appears only if the wrong method is chosen. If that is the case, the following warning appears:

`Unknown drag rise boundary. Check settings!`

If the data provided to the method does not allow the calculation of M_{dd} the second warning present in this method appears as follow:

`The drag divergence Mach number cannot be estimated`

The impossibility to calculate M_{dd} is linked sometimes to the short amount of experimental data given by some of the methods. In some cases this data do not extend long enough to allow the calculation of M_{dd}. This was the case of the Method C of Section 2.3.

8.4.3. UNKNOWN WING WAVE DRAG ESTIMATION METHOD

The method `WingWaveDragTransonic` uses the procedures specified in the settings to calculate the wave drag of the wing. If the method specified do not correspond with any of the available options the following warning appears:

`Unknown wing wave drag estimation method:` *`WingWaveDragMethod`* `Check settings!`

If this is the case, the values of the wave drag coefficient are automatically converted to zero along the whole transonic range.

BIBLIOGRAPHY

[1] E. Torenbeek, *Advanced Aircraft Design* (Wiley, 2013).

[2] ESDU, *A framework relating the drag-rise characteristics of a finite wing/body combination to those of its basic aerofoil*, Tech. Rep. 78009 (ESDU, 1978).

[3] J. D. Anderson, *Fundamentals of aerodynamics*, 5th ed. (McGraw HIll, 2007).

[4] L. M. Nicolai and G. E. Carichner, *Fundamentals of Aircraft and Airship Design*, Vol. I - Aircraft design (AIAA Education Series, 2010).

[5] D. P. Raymer, *Aircraft Design: A Conceptual Approach* (AIAA, 1989).

[6] R. Finck, *USAF stability and control, Datcom* (AF Wright Aeronautical Laboratories, 1978).

[7] R. C. Feagin and W. D. Morrison, *Delta Method, an empirical drag buildup technique*, Tech. Rep. 151971 (NASA, 1978).

[8] J. B. McDevitt, *A correlation by means of transonic similarity rules of experimentally determined characteristics of a series of symmetrical and cambered wings of rectangular planform*, Tech. Rep. 1253 (NACA, 1951).

[9] R. Elmendorp, *Synthesis of novel aircraft concepts for future air travel*, Master's thesis, Delft University of Thechnology (2013).

[10] W. Mason, *Analytic model for technology integration in aircraft design*, AIAA (1990).

[11] C. W. Boppe, *CFD drag prediction for aerodynamic design*, AGARD Advisory Report 256 (1988).

[12] C. N. H. Lock, *The Ideal Drag due to a Shock Wave*, Tech. Rep. 2512 (Aeronautical Research Council, 1945).

[13] W. F. Hilton, *High speed Aerodynamics* (Longmans, Green and Co., 1951).

[14] W. D. Morrison, *Advanced airfoil design empirically based transonic aircraft-drag buildup technique*, Tech. Rep. 137928 (NASA, 1976).

[15] R. P. Johnson, *Minimum drag coefficient of wings*, Tech. Rep. RM-604 (RAND, 1951).

[16] ESDU, *Geometrical properties of cranked and straight-tapered wing planforms*, Tech. Rep. 76003 (ESDU, 1976).

[17] E. Obert, *Aerodynamic Design of Transport Aircraft* (IOS Press, 2009).

[18] ESDU, *Adaptation of drag-rise charts in T.D.Memor.71019 to the mid-semi-span portion of swept and tapered planform*, Tech. Rep. 72027 (ESDU, 1972).

[19] ESDU, *Drag-rise Mach number of aerofoils having a specified form of upper-surface pressure distribution: charts and comments on design*, Tech. Rep. 71019a (ESDU, 1987).

[20] R. S. Shevell, *Fundamentals of flight* (Prentice Hall, 1989).

[21] C. D. Harris, *Aerodynamic characteristics of the 10-percent-thick NASA supercritical airfoil 33 designed for a normal force coefficient of 0.7*, Tech. Rep. X-72711 (NASA, 1975).

[22] C. D. Harris, *Aerodynamic characteristics of the 14-percent-thick NASA supercritical airfoil designed for a normal force coefficient of 0.7*, Tech. Rep. X-72712 (NASA, 1975).

[23] C. D. Harris, *NASA Supercritical Airfoils. A Matrix of Family-Related Airfoils*, Tech. Rep. 2969 (NASA, 1990).

[24] J. C. Ferris, *Static longitudinal aerodynamic characteristics of a model with a modified 17-percent-thick supercritical wing*, Tech. Rep. X-3211 (NASA, 1975).

[25] IHS, *Jane's all the world's aircraft,* janes.ihs.com (2015), retrieved March 30th, 2015.

[26] R. Vos and S. Farokhi, *Introduction to Transonic Aerodynamics* (Springuer, 2015).

[27] J. Tuszynski, *Surface intersection,* www.mathworks.com/matlabcentral/fileexchange/48613 (2014), retrieved March 31th, 2015.

[28] ESDU, *Drag of stub wings and fairings on a flat plate with a turbulent boundary layer at subsonic and supersonic speeds*, Tech. Rep. 84035a (ESDU, 1988).

[29] L. T. Goodmanson and L. B. Gratzer, *Recent advances in aerodynamics for transport aircraft,* AIAA (1973).

[30] J. R. Carlson and M. Lamb, *Integration effects of pylon geometry on a high-wing transport airplane*, Tech. Rep. 2877 (NASA, 1989).

[31] P. M. Sforza, *Commercial airplane design principles* (Butterworth-Heinemann, 2014).

[32] I. H. Abbott and A. E. von Doenhoff, *Theory of wings and sections* (McGraw Hill, 1959).

[33] R. T. Whitcomb, *A study of the zero-lift drag-rise characteristics of wing-body combinations near the speed of sound*, Tech. Rep. 1273 (NACA, 1952).

[34] TU Delft, *Synthesis/Initiator,* http://fppwiki.lr.tudelft.nl/index.php/Synthesis/Initiator (2015), retrieved May 8th, 2015.